1

Field-Flow Fractionation Techniques

P. Stephen Williams

Cambrian Technologies Inc., 1772 Saratoga Avenue, Cleveland, OH, 44109, USA

1.1 Introduction

Field-flow fractionation (FFF) comprises several related techniques for the separation and characterization of macromolecular, colloidal, and particulate materials. All of the FFF techniques have in common the requirement of a non-uniform, laminar flow of a carrier fluid and a means of inducing different sample species to be distributed differently within the flow, resulting in their different migration velocities and thereby their separation. Non-uniform laminar fluid velocity profiles are easily obtained when fluid flows under the influence of pressure through thin parallel-plate, annular, or tubular channels. Fluid velocity approaches zero at the stationary walls due to viscous drag and approaches a maximum velocity farthest from the walls. The transport of sample species across the velocity profiles in such channels, perpendicular to the direction of flow, can be accomplished in a number of different ways, each giving rise to a different member of the FFF family.

The transport of macromolecular and colloidal species toward the accumulation wall causes an increase in concentration adjacent to the wall, which, for these submicron species, is opposed by diffusion. This results in a steady-state distribution next to the wall, the thickness of which is a function of the species properties and the applied field. Diffusion is negligible for supramicron species, and their transport to the accumulation wall is opposed by hydrodynamic lift forces within the shear flow close to the wall (Caldwell et al. 1979; Williams et al. 1992, 1994, 1996b). In either case, species that differ in their rate of transverse transport to the wall and/or in their rate of opposing transport, or that differ in the position-dependent transverse forces they experience, quickly approach different steady-state concentration distributions within the shear flow close to the accumulation wall. This results

Field-Flow Fractionation: Principles and Applications, First Edition.
Edited by Céline Guéguen, Mohammed Baalousha, and S. Kim R. Williams.
© 2026 WILEY-VCH GmbH. All rights reserved, including rights for text and data mining and training of artificial intelligence technologies or similar technologies. Published 2026 by WILEY-VCH GmbH.

in their different mean migration velocities along the channel. The rapid Brownian exchange of positions of identical particles within a thin particle distribution results in their migration as a coherent zone. Different species are consequently separated as they migrate along the length of the channel, and a detector at the channel outlet can be used to observe their elution as a function of time. The theoretical underpinnings of the separation mechanisms of FFF are not the focus of this chapter. These have been discussed in earlier works by Martin and Williams (1992), Martin (1998), and Williams (2022).

The transport of species across the channel thickness can be achieved by various means. For example, a field that interacts with some material property of the sample species may be applied transversely across the channel thickness. Fields such as the Earth's gravitational field or a centrifugal field induce the sedimentation of species that are denser than the carrier fluid. This type of field is used in the gravitational FFF (GrFFF) and sedimentation FFF (SdFFF) (also known as centrifugal FFF or CF3) techniques, respectively. Electric, dielectric, and magnetic fields have been employed in electrical FFF (ElFFF), dielectrical or dielectrophoretic FFF (DEP-FFF), and magnetic FFF (MgFFF). A temperature gradient maintained across the channel thickness can induce the transport of macromolecules and colloids, generally toward the colder wall. This temperature-gradient-induced transport is known as thermal diffusion or thermophoresis, the mechanisms of which continue to be investigated. Such a thermal gradient is used in thermal FFF (ThFFF).

A technique of FFF that does not make use of a field or gradient to drive species to the accumulation wall is known as flow FFF (FlFFF). This form employs a secondary component of flow through a semipermeable accumulation wall (permeable only to the fluid) that carries all species to the wall at the same rate by entrainment in this transverse component of fluid flow. The rate of transport is non-selective and does not depend on the size or on any material properties of the sample species. It is only differences in the opposing rates of diffusional transport or in hydrodynamic lift forces that give rise to different distributions in the non-uniform component of flow along the channel length and hence different elution times.

Table 1.1 lists the equations for the retention parameter λ for submicron species (approximately equal to the ratio of mean distribution thickness to the channel thickness) for the different FFF techniques considered in this chapter, along with the different physicochemical sample properties that influence the parameter and therefore retention. In each case, the measurement of retention time can potentially allow the calculation of the respective retention parameter, and hence the determination of a listed sample property, given knowledge of all other relevant parameters.

Other types of fields have been proposed for use in FFF, such as acoustic, photophoretic, etc., but these are not presently in common use and will not be discussed in this chapter.

Table 1.1 FFF Techniques with Respective Retention Parameter Equations and the Sample Physicochemical Properties that Control Retention. (The explanation of symbols may be obtained in the respective sections of the chapter.)

Sample properties	
AsFlFFF, HF-FFF	
$\lambda_0 = \frac{DV^0}{\dot{V}_c w^2} = \frac{kTV^0}{f\dot{V}_c w^2} = \frac{kTV^0}{3\pi\eta d_h \dot{V}_c w^2}$	D, f, d_h
GrFFF, SdFFF	
$\lambda = \frac{kT}{V_p \Delta\rho G w} = \frac{6kT}{\pi d^3 \Delta\rho G w}$	$V_p, \Delta\rho, \rho_p$
ThFFF	
$\lambda = \frac{D}{D_T(\mathrm{d}T/\mathrm{d}x)w} = \frac{T}{\alpha(\mathrm{d}T/\mathrm{d}x)w}$	D, D_T, α
ElFFF	
$\lambda = \frac{D}{\mu_e E_{\mathrm{eff}} w} = \frac{kT}{3\pi\eta d_h \mu_e E_{\mathrm{eff}} w}$	D, μ_e, d_h
MgFFF	
$\lambda = \frac{\mu_0 kT}{V_m \Delta\chi B \nabla B w} = \frac{kT}{V_m M \nabla B w} = \frac{6kT}{\pi {d_m}^3 M \nabla B w}$	$V_m, \Delta\chi, M, d_m$

1.2 Flow Field-Flow Fractionation

Parallel-plate channel flow FFF (FlFFF) was introduced in 1976 (Giddings et al. 1976c; Giddings et al. 1976d; Lee and Lightfoot 1976). It was originally implemented using channels having two permeable frit walls. A semipermeable ultrafiltration membrane covering one of the walls served as the accumulation wall. The membrane is permeable to the fluid but not to the sample materials. It was pushed into contact with the supporting frit due to its hydraulic resistance to the flow passing through it. An equal flow was introduced to the channel *via* the permeable depletion frit wall. It was assumed that the cross-flow velocity component was constant throughout the channel and that the sample species were eluted along the length of the channel under the influence of a constant volumetric channel flow rate. However, actual conditions in the channel may deviate from this ideal model. The hydraulic resistance of the membrane is likely to be sufficiently high that the pressure drop along the channel length would not significantly influence the local flux through the membrane. This may not be the case for the depletion frit wall, however, and there is a possibility that the pressure drop along the channel

may influence the local flow through the depletion wall. The frit porosity may also vary along its length or its breadth. These effects may cause the mean channel flow velocity to vary along the channel length, with a deviation of void time and elution times from those predicted from theory based upon the assumption of ideal conditions (Martin and Hoyos 2011). Although this design was used with success for many years, it has now been largely superseded by asymmetrical FlFFF (AsFlFFF or AF^4).

AsFlFFF was proposed independently by Granger et al. (1986) and by Wahlund and Giddings (1987), with much of the subsequent early development being carried out by Wahlund and co-workers. In this form of FlFFF, the permeable depletion wall is replaced by an impermeable wall, such as a plane glass plate, which eliminates the uncertainties associated with the frit flow. A fraction of the fluid entering the channel inlet exits through the accumulation wall and the remainder *via* the channel outlet. The gradual loss in volumetric flow along the length of the channel is partially compensated by a reduction in the channel breadth from inlet to outlet. This reduction in channel breadth is typically linear (Litzén and Wahlund 1991; Litzén 1993) or, less commonly, exponential (Ahn et al. 2010; Williams 1997). The purpose is to avoid the situation where mean fluid velocity falls to such a low level close to the channel outlet that sample immobilization on the membrane might occur (Wahlund et al. 1986; Williams 2000b). An exploded view of an AsFlFFF channel is shown in Figure 1.1.

Channels are typically between 25 and 35 cm long, 2.5–3.0 cm wide close to the inlet, and less than 1.0 cm wide close to the outlet. Spacer thicknesses of 250–350 μm are commonly used. Smaller channels, having lengths of less than 10 cm and widths of less than 1.0 cm at the inlet narrowing to less than 0.2 cm at the outlet, are also in use. Their advantages and disadvantages have been compared (You et al. 2017). As in all forms of FFF, the carrier fluid composition must minimize

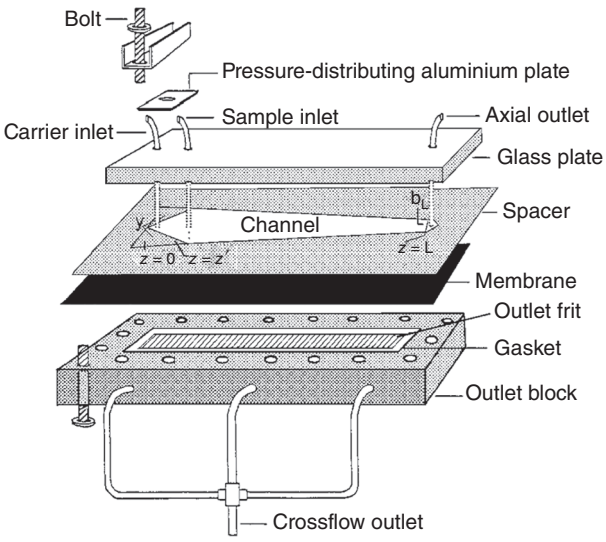

Figure 1.1 Exploded view of the components of an AsFlFFF channel. *Source*: Schimpf et al. (1997) / John Wiley & Sons.

particle–particle and particle–wall or membrane interaction. This is accomplished with the use of a suitable surfactant and adjustment of ionic strength and pH (Gopalakrishnan et al. 2023; Hansen and Giddings 1989; Hansen et al. 1989; Moon 1995; Nickel et al. 2021).

In AsFlFFF, the retention parameter for the normal mode of elution is given by

$$\lambda_0 = \frac{D}{|u_0|\,w} = \frac{DV_C^0}{\dot{V}_c w^2} = \frac{kTV_C^0}{3\pi\eta\dot{V}_c w^2 d_h} \tag{1.1}$$

where D is the diffusion coefficient, $|u_0|$ is the magnitude of the transverse component of fluid velocity adjacent to the membrane surface, w is the channel thickness, V_C^0 is the volume of the channel, $\dot{V}_c$ is the volumetric cross-flow rate through the membrane, k is Boltzmann's constant, T is the absolute temperature, η is the fluid viscosity, and d_h is the hydrodynamic diameter of the species. The final form on the right of Eq. (1.1) makes use of the Stokes–Einstein equation for diffusion coefficient: $D = kT/f$ where f is the friction coefficient, equal to $3\pi\eta d_h$. The subscript 0 on λ_0 and $|u_0|$ refers to the distance $x = 0$ from the accumulation wall. It is included because in AsFlFFF, the cross-flow velocity varies from a maximum u_0 at the membrane to zero at the depletion wall (Wahlund and Giddings 1987). The variation of $|u|$ across the channel thickness is shown by the full curve in Figure 1.2. It is assumed that membrane flux, and therefore $|u_0|$, is constant over its surface, which requires uniform hydraulic resistance, and the pressure drop along the channel length to be much smaller than the pressure drop across the membrane thickness.

For the classical model of FFF where the field-induced transverse velocity is constant, resulting in exponential concentration profiles, and the velocity profile is parabolic across the channel thickness, the retention ratio R, equal to the ratio of particle zone velocity to mean fluid velocity, is given by (Giddings 1978)

$$R = 6\alpha(1-\alpha) + 6\lambda\left\{(1-2\alpha)\coth\left(\frac{1-2\alpha}{2\lambda}\right) - 2\lambda\right\} \tag{1.2}$$

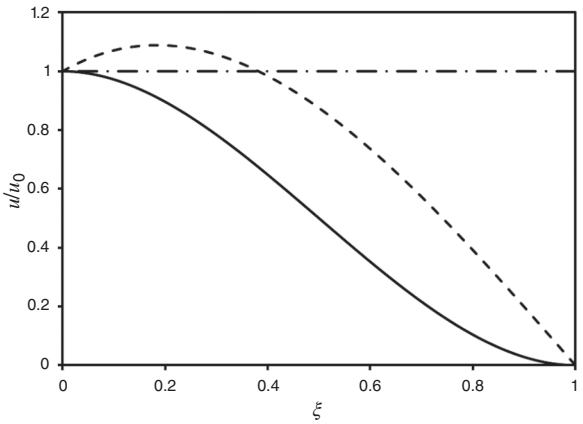

Figure 1.2 Transverse component of fluid velocity u relative to the velocity at the accumulation wall u_0 as a function of the fractional distance across the channel thickness ξ for AsFlFFF (full curve), HF-FFF (dashed curve), and classical FFF, such as ideal symmetrical FlFFF (dash-dotted line). For HF-FFF, $\xi = 1 - \rho = 1 - r/r_f$ so that $\xi = 1$ at the axis.

which, for R less than about 0.5 (which encompasses the most effective range of retention and separation), is very well approximated by

$$R = 6\alpha(1-\alpha) + 6\lambda(1-2\alpha-2\lambda) \tag{1.3}$$

In Eqs. (1.2) and (1.3), α is a first-order correction for finite particle size, and for a spherical particle, α is equal to $d/2w$ where d is the particle diameter. It accounts for the fact that the center of a spherical particle is sterically excluded from regions of the channel within a radius of the walls.

In the FFF analysis of submicron species, the unavoidable, and often dominant, source of bandspreading is due to the nonequilibrium effect (Giddings 1968; Giddings et al. 1975). The rapid exchange of particle positions within a thin particle distribution was mentioned as resulting in coherent migration as a narrow zone. The finite time taken for the position exchange gives rise to this nonequilibrium bandspreading. This contribution to bandspreading may be described in terms of a nonequilibrium plate height given by

$$H = \frac{\chi w^2 \langle v \rangle}{D} \tag{1.4}$$

in which χ is the nonequilibrium bandspreading parameter and $\langle v \rangle$ is the mean channel flow velocity. Including the first-order correction for particle size, the product of R and χ for the classical model of FFF is given by (Giddings 1978, 1979; Williams and Giddings 1994)

$$\begin{aligned}\chi R = 12\lambda^2 \big[&\{336\lambda^4 + 24(1-2\alpha)^2\lambda^2 - (1-2\alpha)^4\} \\ &- \{120(1-2\alpha)\lambda^3 - 6(1-2\alpha)^3\lambda\} \coth\left((1-2\alpha)/2\lambda\right) \\ &- \{12(1-2\alpha)^2\lambda^2 - (1-2\alpha)^4\} \coth^2\left((1-2\alpha)/2\lambda\right) \\ &-6(1-2\alpha)^3\lambda \coth^3\left((1-2\alpha)/2\lambda\right)\big]\end{aligned} \tag{1.5}$$

which, for R less than about 0.5, is very well approximated by

$$\chi R = 144\lambda^4((1-2\alpha)^2 - 10(1-2\alpha)\lambda + 28\lambda^2) \tag{1.6}$$

The variation of cross-flow velocity across the channel thickness in AsFlFFF results in a deviation of the concentration profile for each species from an exponential. As a consequence, both the retention ratio R and the nonequilibrium bandspreading parameter χ deviate from the solutions given in Eqs. (1.2–1.6) (Wahlund and Giddings 1987; Williams 2015). These deviations are significant at relatively low retention levels. For example, assuming $\alpha = 0$, R is more than 11% greater than predicted for the classical model of FFF at $\lambda_0 = 0.12$, but less than 4% greater at $\lambda_0 = 0.05$. The magnitude of χ is more than 72% greater in AsFlFFF for $\lambda_0 = 0.12$, more than twice as high for $\lambda_0 = 0.08$, and 59% higher at $\lambda_0 = 0.05$ (Williams 2015). The differences are much smaller for stronger retention levels. A tabulation of R, χ, and χR for AsFlFFF for λ_0 from 0.0001 to 1024 can be found in the Electronic Supplementary Material associated with Williams (2017).

Prediction of elution times in isocratic (constant flow rate) AsFlFFF, and conversely, the calculation of retention ratio R from which λ_0 and hence d_h may be extracted, requires knowledge of the void time t^0, the time for a non-retained

material to pass along the channel from the start of elution to the channel outlet. In AsFlFFF, as in the other FFF techniques, elution does not generally commence from the channel inlet. The starting point depends on the procedure followed to introduce and relax the sample. Sample relaxation close to the steady-state concentration profiles prior to elution is necessary so as to obtain retention consistent with steady-state theory and not introduce avoidable bandspreading.

The methods of sample introduction and relaxation in AsFlFFF generally make use of opposing fluid flow in the channel. In the original implementation (Wahlund and Giddings 1987), fluid is introduced to the channel inlet at a low flow rate, while a higher flow is introduced at the port that serves as the channel outlet during sample elution. All introduced fluid exits through the membrane at this stage. With the loss of fluid through the membrane, the mean fluid velocity decreases from both channel inlet and outlet toward a point in the channel close to the inlet determined by the ratio of the two introduced flow rates. The sample is then introduced into the flow at the channel inlet, whereupon it is carried to the focusing point where it is allowed to relax to a steady-state distribution against the membrane. The converging flows ensure that the sample is focused into a narrow zone as it relaxes. Elution commences when the inflow at the channel outlet is removed, the channel inlet flow rate is increased, and a fraction of this inlet flow is allowed to exit at the channel outlet. This method was improved upon by the downstream central injection method introduced by Wahlund and Litzén (1989). In this method, the focusing flow rates to the channel inlet and outlet are applied as in the initial approach, but the sample is introduced to a port through the impermeable depletion wall close to the sample focusing point. After sufficient time for focusing and relaxation of the sample, the flow regime for sample elution is imposed as in the original method. The disadvantage of the original method lies in the fact that the sample enters the channel inlet and is initially distributed across the full channel thickness. A fraction of the sample is therefore already close to the membrane at the inlet, and this fraction must migrate by the FFF mechanism to the focusing point at a reduced velocity. The result is that a longer focusing time is necessary for the original method as compared to the downstream central injection method. Long focusing times are to be avoided as they can result in aggregation of some analytes or can lead to sample loss through adsorption on the membrane surface at the focusing point (Wahlund 2013). The downstream central injection method also has the advantage of confining the sample to the central region of the channel, away from the channel edges. In either case, elution starts at the focusing point and ends at the channel outlet, and the effective void volume for elution V^0 is therefore smaller than the channel volume V_C^0 and is given by

$$V^0 = \frac{\dot{V}_B}{\dot{V}_F + \dot{V}_B} V_C^0 \tag{1.7}$$

where $\dot{V}_B$ and $\dot{V}_F$ are the backward and forward focusing flow rates. It can then be shown (Williams 2016) that the void time is given by

$$t^0 = \frac{V_C^0}{\dot{V}_c} \ln\left(\frac{\dot{V}_B\dot{V}_0 + \dot{V}_F\dot{V}_L}{(\dot{V}_F + \dot{V}_B)\dot{V}_L}\right) \tag{1.8}$$

where $\dot{V}_0$ is the flow rate at the channel inlet and $\dot{V}_L$ is the channel outlet flow rate under elution conditions, so that $\dot{V}_c = \dot{V}_0 - \dot{V}_L$.

Further improvement to sample loading and focusing in AsFlFFF has been made where the reverse focusing flow is introduced to the channel *via* a second port in the impermeable depletion wall at a point between the focusing point and the channel outlet (Messaud et al. 2009). If the channel outlet is closed during sample introduction and focusing, then the focusing point would be unchanged. However, there is now the option of allowing a fraction of this focusing flow to exit at the channel outlet during the focusing period. Suppose that during focusing, the flow rate at the channel inlet is represented by $\dot{V}_{0(f)}$ (equivalent to $\dot{V}_F$ in the treatment above), the flow rate at the outlet by $\dot{V}_{L(f)}$, and the focusing flow rate at the second port in the depletion wall by $\dot{V}_{\text{focus}}$. Then, it follows that the cross-flow rate through the membrane during focusing, $\dot{V}_{c(f)}$ is given by $\dot{V}_{0(f)} + \dot{V}_{\text{focus}} - \dot{V}_{L(f)}$. It can then be simply shown that

$$V^0 = \left(\frac{\dot{V}_{\text{focus}} - \dot{V}_{L(f)}}{\dot{V}_{c(f)}} \right) V_C^0 = \left(\frac{\dot{V}_{c(f)} - \dot{V}_{0(f)}}{\dot{V}_{c(f)}} \right) V_C^0 \tag{1.9}$$

and that the effective void time is given by

$$t^0 = \frac{V_C^0}{\dot{V}_c} \ln \left(\frac{(\dot{V}_{c(f)} - \dot{V}_{0(f)})\dot{V}_0 + \dot{V}_{0(f)}\dot{V}_L}{\dot{V}_{c(f)}\dot{V}_L} \right) = \frac{V_C^0}{\dot{V}_c} \ln \left(1 + \frac{V^0}{V_C^0} \frac{\dot{V}_c}{\dot{V}_L} \right) \tag{1.10}$$

in which $\dot{V}_0$, $\dot{V}_L$, and $\dot{V}_c$ are the channel inlet, outlet, and cross-flow rates during elution, respectively. The great advantage of this method is that focusing conditions may be set up such that $\dot{V}_{L(f)} = \dot{V}_L$ and $\dot{V}_{c(f)} = \dot{V}_c$. The initiation of elution would then be accomplished simply by diverting the focusing flow rate $\dot{V}_{\text{focus}}$ to augment the flow rate $\dot{V}_{0(f)}$ at the inlet so that $\dot{V}_0 = \dot{V}_{0(f)} + \dot{V}_{\text{focus}}$. This rerouting of flow would be achieved with very little disturbance to channel internal pressure, little disturbance to the flow through the detector, and therefore little disturbance to baseline response.

An alternative method of sample introduction and relaxation known as the frit-inlet method has also proven to be quite successful. This is a method similar to the split-inlet method of hydrodynamic sample relaxation proposed by Giddings (1985) and later implemented in SdFFF (Lee et al. 1989). Hydrodynamic relaxation has the advantage that a stop-flow period for sample relaxation is not required because the sample is carried to the region adjacent to the accumulation wall by a merging of two fluid streams at the channel inlet. It was proposed by Giddings (1990a) that such a hydrodynamic relaxation could be obtained conveniently in symmetrical FlFFF by introducing the majority of the channel flow through a separate, small frit element in the depletion wall placed across the full channel breadth, just beyond the channel inlet, while the sample entered at the channel inlet. The drawback is that the finite sample volume enters at a reduced flow rate, which broadens the initial zone. On the other hand, if the sample flow rate is not a small fraction of the total channel flow rate, then there will be a contribution to bandspreading due to the residual relaxation (Liu et al. 1991). It has been shown using computational fluid dynamics modeling that the relaxation under a frit-inlet

element is a little more complicated than this discussion might imply, and that there is an additional small contribution to bandspreading (Vauthier and Williams 1998).

Moon and coworkers soon showed that this frit-inlet technique could be used successfully in AsFlFFF for isocratic operation (Moon et al. 1997; Moon et al. 1999) and for programmed decay of cross-flow rate (Kim et al. 2018; Lee et al. 2005; Moon 2001; Moon et al. 2002). It was pointed out by Moon et al. (1999) that the earlier treatments of optimization of the ratio of sample flow to frit flow rates had not taken into account the flow through the membrane below the frit element. When this is considered, it is apparent that the problem of residual relaxation can be eliminated simply by ensuring that

$$\dot{V}_s \leq \dot{V}_c \frac{A_f}{A_C} \tag{1.11}$$

where $\dot{V}_s$ is the flow rate at the channel inlet into which the sample is introduced, A_f is the area of the frit element in the depletion wall, and A_C is the total area of the membrane accumulation wall so that $V_C^0 = A_C w$, and it is assumed that the flux through the membrane is uniform throughout the channel. If the sample flow rate $\dot{V}_s$ is set equal to $\dot{V}_c(A_f/A_C)$, then Moon et al. (1999) showed that the effective void time, if this is assumed to be measured from the downstream edge of the frit element to the channel outlet, is given by

$$t^0 = \frac{V_C^0}{\dot{V}_c} \ln\left(\frac{\dot{V}_f}{\dot{V}_L}\right) = \frac{V_C^0}{\dot{V}_c} \ln\left(\frac{\dot{V}_f}{\dot{V}_s + \dot{V}_f - \dot{V}_c}\right) \tag{1.12}$$

where $\dot{V}_f$ is the flow rate through the frit element and $\dot{V}_L \dot{V}_L$ is the channel outlet flow rate, which the final expression on the right of Eq. (1.12) shows is equal to $\dot{V}_s + \dot{V}_f - \dot{V}_c$. The non-retained time beneath the frit element t_f^0 is then given by

$$t_f^0 = \frac{\dot{V}_s}{\dot{V}_f - \dot{V}_s} \frac{V_C^0}{\dot{V}_c} \ln\left(\frac{\dot{V}_f}{\dot{V}_s}\right) \tag{1.13}$$

If a sample species was indeed non-retained beneath the frit element, then the retention ratio R would be given by $t^0/(t_r - t_f^0)$, where t_r is the observed elution time for the whole channel. However, the fraction of the sample that enters the channel close to the membrane would be retarded to some extent, which would lead to a small error if R were to be calculated in this way. Nevertheless, the stop-less, frit-inlet technique is extremely convenient, and the errors probably negligible when conditions are properly set up. The frit-inlet method of sample introduction has been compared with the focusing method for linearly programmed cross-flow operation in terms of sample recovery, efficiency, resolution, and overloading for a range of different samples and operating conditions (Fuentes et al. 2019).

It has been shown how both retention times and fractionating power may be predicted for constant and programmed decay of cross-flow rate in AsFlFFF (Williams 2016, 2017, 2024). The fractionating power is a measure of relative resolving power and indicates the quality of the separation that can be expected for a polydisperse sample as a function of particle size or molecular weight (Giddings et al. 1987). It was also shown that, for a polydisperse sample, the residual

polydispersity in the channel outlet stream is predicted to be approximately equal to the reciprocal of four times the fractionating power. The optimization of experimental conditions for polydisperse sample analysis in FFF should logically be based on achieving some acceptable level of fractionating power across the full range of the sample. It can then be ensured that every part of the sample is well fractionated, and if light scattering detection is used as a secondary determinant of particle size or molecular weight, then the data returned are not skewed by excessive outlet polydispersity. The use of light scattering characterization in conjunction with the optimization of flow conditions for good fractionation is therefore complementary. The light scattering characterization corrects for small departures from FFF theory (such as those due to particle–membrane and particle–particle interactions) and uncertainties in instrument parameters (such as channel thickness, channel volume, carrier fluid temperature and viscosity, etc.), while the fractionating power calculations ensure that conditions are conducive to good fractionation.

It is often assumed that nonequilibrium bandspreading is the dominant cause of bandspreading in FFF. However, it has long been noted that the observed efficiencies in FlFFF are generally lower, and often much lower, than are predicted for the nonequilibrium effect alone (Giddings et al. 1976c; Litzén 1993; Litzén et al. 1993; Litzén and Wahlund 1991). Carlshaf and Jönsson (1993) had suggested that variation in porosity in hollow fiber FFF (HF-FFF) could cause bandspreading. The excess bandspreading in FlFFF may also be the result of small variations in channel thickness, due to the membrane surface not being perfectly planar, as well as small variations in membrane hydraulic resistance. These features can together give rise to a multipath contribution. It has been shown how this effect could be included in the calculation of fractionating power in AsFlFFF (Williams 2016, 2017). In the case of programmed AsFlFFF, it was assumed that the multipath effect does not change significantly with cross-flow rate and does not vary significantly along the length of the channel (Williams 2017). (Of course, in practice there may be some variation in each case.) The calculations could then be carried out for any programmed variation of cross flow rate with time, with either channel outlet flow rate or inlet flow rate held constant, or for any arbitrary variation of cross-flow rate, outlet flow rate, and inlet flow rate. This means that it is possible to carry out the calculations necessary to transform a fractogram obtained under arbitrary, but monitored, flow rates into a particle size or molecular weight distribution (Williams et al. 2001).

1.3 Hollow-Fiber Field-Flow Fractionation

Hollow fiber FFF (HF-FFF) has much in common with AsFlFFF, but it utilizes a semipermeable capillary tube or fiber rather than a flat channel. The fiber is mounted inside a mantle, such as a glass tube. Carrier fluid is pumped into the fiber, while suction is applied to the mantle so that a fraction of the fluid exits

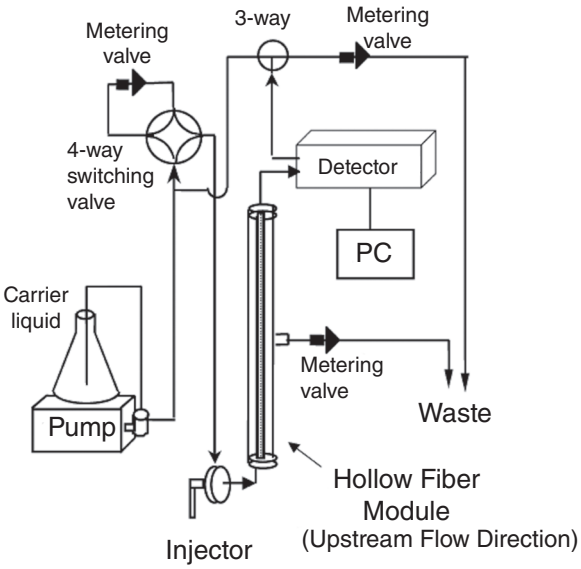

Figure 1.3 Schematic of the components of a HF-FlFFF system. *Source*: Min et al. (2002) / with permission of ELSEVIER.

through the fiber wall and the remainder through the fiber outlet. The species to be separated are carried to the fiber walls by the radial velocity component of the fluid. A schematic of an HF-FFF system is shown in Figure 1.3. The technique was in fact described before symmetrical FlFFF by Lee et al. (1974) and by Doshi et al. (1975).

In the simplified theoretical treatment considered here, we shall assume that the pressure drop along the fiber is small relative to that across the fiber wall. It has been shown by Lee et al. (1999) that this is a reasonable assumption for typical polysulfone fibers (molecular weight cutoff of 30 kDa and permeability of 0.415 cm/min atm). The mean velocity along the fiber then falls linearly with the distance from the inlet according to

$$\langle v_z \rangle = \langle v_0 \rangle - \frac{\dot{V}_c}{\pi {r_f}^2} \frac{z}{L} \tag{1.14}$$

where $\langle v_z \rangle$ is the mean fluid velocity at distance z from the inlet, $\langle v_0 \rangle$ is the mean velocity at the inlet, $\dot{V}_c$ is the volumetric flow rate through the fiber wall, r_f is the internal radius of the fiber, and L is the length of the fiber. The radial component to fluid velocity u inside the fiber is given by

$$u = u_0 \rho (2 - \rho^2) \tag{1.15}$$

where u_0 is the radial velocity at the wall, assumed to be constant along the length of the fiber, and ρ is the ratio of radial distance r from the axis to the internal radius r_f

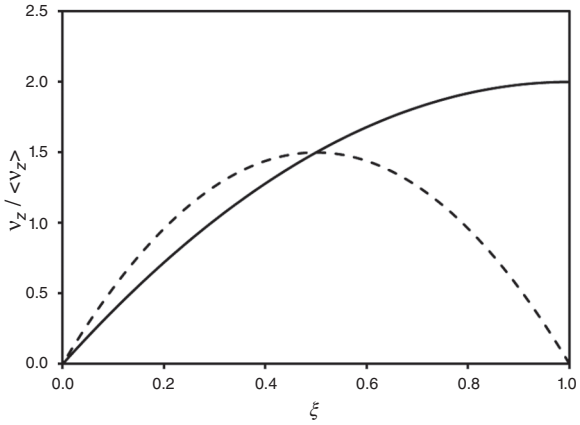

Figure 1.4 Longitudinal fluid velocity component v_z at distance z from the inlet relative to mean velocity $\langle v_z \rangle$ as a function of the fractional distance across the channel ξ for HF-FFF (full curve) and parallel plate FFF (dashed curve). For HF-FFF, $\xi = 1 - \rho = 1 - r/r_f$ so that $\xi = 1$ at the axis.

of the fiber. The radial velocity component therefore passes through a maximum of 1.089 u_0 at $\rho = 0.8165$ as shown by the dashed curve in Figure 1.2. Also shown for comparison are the transverse velocity components for AsFlFFF (the full curve) and the classical model of FFF in which the velocity is constant (the dash-dotted horizontal line). The horizontal axis is given in terms of relative distance ξ from the accumulation wall, so that in HF-FFF, $\xi = (1 - \rho) = (1 - r/r_f)$, and in planar channel FFF, $\xi = x/w$.

The longitudinal velocity profile in the hollow fiber at a distance z from the inlet is given by

$$v_z = 2\langle v_z \rangle (1 - \rho^2) \tag{1.16}$$

This is shown in Figure 1.4 as the full curve with the parabolic profile for planar channels (dashed curve) included for comparison.

The opposition of diffusion to the buildup of concentration close to the wall due to radial transport according to Eq. (1.15) results in a concentration profile in HF-FFF given by

$$c = c_0 \exp\left(-\frac{1}{\lambda_0}\left(\frac{3}{4} - \rho^2 + \frac{\rho^4}{4}\right)\right) \tag{1.17}$$

where c_0 is the concentration at the outer wall and, analogous to the case of AsFlFFF, the value of λ_0 is related to conditions at the accumulation wall so that $\lambda_0 = D/|u_0|r_f$. Lee et al. (1974) showed that, when the longitudinal fluid velocity profile of Eq. (1.16) is imposed, the retention ratio is given by

$$R = \frac{4{\lambda_0}^{0.5}(\exp(-1/4\lambda_0) - \exp(-1/\lambda_0))}{\pi^{0.5}\left(\operatorname{erf}\left({\lambda_0}^{-0.5}\right) - \operatorname{erf}\left(0.5{\lambda_0}^{-0.5}\right)\right)} - 2 \tag{1.18}$$

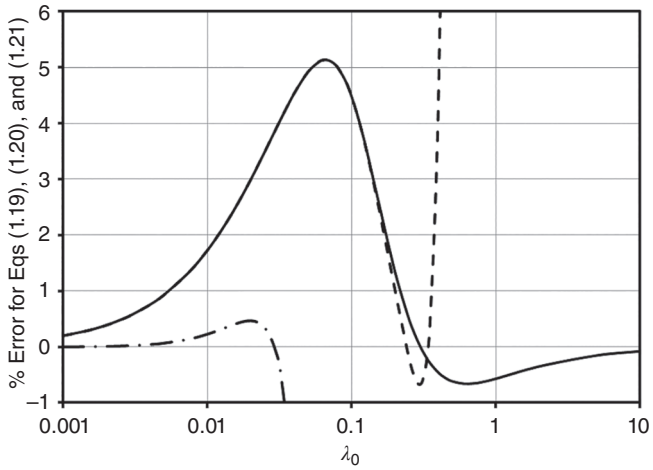

Figure 1.5 The percent error associated with (Eqs. 1.19–1.21) for R in HF-FFF compared to the accurate solution given by Eq. (1.18), plotted as the full curve, dashed curve, and dash-dotted curve, respectively.

For the approximation of an exponential concentration profile, Lee et al. (1999) showed that

$$R \approx \frac{4\lambda_0\left(1 - 3\lambda_0 + 3\lambda_0^2 + \left(0.5 - 3\lambda_0^2\right)\exp(-1/\lambda_0)\right)}{1 - \lambda_0 + \lambda_0\exp(-1/\lambda_0)} \tag{1.19}$$

which for small λ_0 is given, to a good approximation, by

$$R \approx \frac{4\lambda_0\left(1 - 3\lambda_0 + 3\lambda_0^2\right)}{(1 - \lambda_0)} \tag{1.20}$$

The error of Eq. (1.19) as compared to the accurate Eq. (1.18) as a function of λ_0 is shown in Figure 1.5 as a full black curve. The retention ratio is overestimated by 1.72% at $\lambda_0 = 0.01$, $R = 0.03854$, and by 2.99% at $\lambda_0 = 0.02$, $R = 0.07460$. The error reaches a maximum of 5.14% at $\lambda_0 = 0.066$, $R = 0.2191$, after which it decreases. The error of Eq. (1.20) is shown as the dashed curve in Figure 1.5. Equation (1.20) behaves almost as well as Eq. (1.19) up to $\lambda_0 = 0.35$, $R = 0.6812$ where R is overestimated by only 0.38%. At $\lambda_0 = 0.4$, $R = 0.7154$, the error rises to 4.37% and increases rapidly beyond that point. It can be seen that Eq. (1.20) has reasonable accuracy (better than 5.2%) for the range of interest. Incidentally, Doshi et al. (1975) derived a series solution for R that is accurate to better than 0.5% up to $\lambda_0 = 0.02$ but is highly inaccurate for larger λ_0. Their solution is given by

$$R = 4\lambda_0\left(1 - 4\lambda_0 + 72\lambda_0^2 - 1485\lambda_0^3 + \cdots\right) \tag{1.21}$$

and the error for this equation is shown as the dash-dotted curve in Figure 1.5.

Steric exclusion may be accounted for by consideration of only the region of the fiber accessible to particle centers (ρ from zero to $1 - \alpha$, where α is the ratio of the

exclusion distance $d/2$ to r_f). For the approximation of an exponential concentration profile, the following result is obtained

$$R \approx \frac{4(\lambda_0+\alpha)\left(1-3\lambda_0+3\lambda_0^2\right)-2\alpha^2(3-3\lambda_0-\alpha)+2\lambda_0\left(1-6\lambda_0^2\right)\exp(-(1-\alpha)/\lambda_0)}{1-\lambda_0-\alpha+\lambda_0\exp(-(1-\alpha)/\lambda_0)}$$
$$\approx \frac{4(\lambda_0+\alpha)\left(1-3\lambda_0+3\lambda_0^2\right)-2\alpha^2(3-3\lambda_0-\alpha)}{1-\lambda_0-\alpha} \tag{1.22}$$

Of course, for practical ranges of R, the exponential terms may be deleted without significant loss of accuracy (as for Eq. (1.20)), as shown by the second solution. It is recommended that for precise calculations, numerical approaches to calculation be followed.

The theory for the nonequilibrium bandspreading effect in HF-FFF has not been as fully developed as for AsFlFFF. Doshi et al. (1975) described sample species migration in HF-FFF in terms of unsteady convective diffusion, and bandspreading was determined to be equivalent to a nonequilibrium bandspreading parameter χ given by the series solution

$$\chi = 16\lambda_0^3(1-24\lambda_0+\cdots) \tag{1.23}$$

which does not account for finite particle size. Only the first term of the series expansion was given and the solution is therefore valid only for $\lambda_0 << 1$.

The sample loading and focusing in HF-FFF is carried out as in the original method for AsFlFFF; downstream loading is not possible. The sample is introduced at the fiber inlet, and it is focused using opposing flows from the inlet and outlet. The effective void volume and void time are calculated using Eqs. (1.7) and (1.8), respectively. The fiber volume V_C^0 must be determined experimentally using non-retained samples if quantitative characterization of sample species is required. This is due to uncertainty in the fiber's internal radius. Alternatively, calibration using standards may be carried out.

1.4 Gravitational Field-Flow Fractionation

Gravitational FFF(GrFFF) was first demonstrated by Berg et al. (1967). They used a flow of fluid in an open channel rather than a conventional closed FFF channel. The conventional form was introduced in 1978 by Giddings and Myers (1978). These channels are the simplest to construct of the different FFF techniques. A spacer out of which the shape of the channel is excised is simply sandwiched between plane glass or Lucite plates. The plates are compressed together using nuts and bolts with the inclusion of a suitable protective support in the case of glass plates. Ports must be bored through one of the glass or Lucite plates to carry fluid to and from the channel. The general construction is illustrated in Figure 1.6.

The gravitational force F_G on a particle in suspension is given by $F_G = V_p \Delta\rho G$, in which V_p is the volume of the particle, $\Delta\rho$ is the difference in density between that of the particle ρ_p and that of the fluid ρ_f ($= \rho_p - \rho_f$), and G is the acceleration

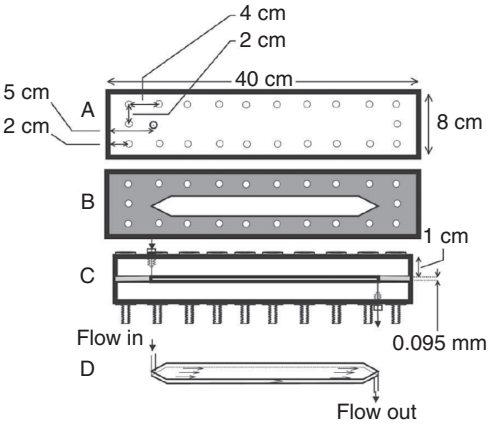

Figure 1.6 Components of a GrFFF channel. A) Lucite blocks, B) Spacer, C) Assembled channel, and D) Schematic representation of the flow channel. *Source*: Beckett et al. (2007) / American Chemical Society.

due to gravity. The sedimentation velocity u is then given by $u = F_G/f$ where f is the friction coefficient equal to $3\pi\eta d_h$ for a particle of hydrodynamic diameter d_h, and where η is the viscosity of the fluid. Recalling Eq. (1.1) we see that

$$\lambda = \frac{D}{|u|w} = \frac{kT}{f}\frac{f}{F_G w} = \frac{kT}{V_p \Delta\rho G w} \tag{1.24}$$

It can be seen from Eq. (1.24) that because gravitational acceleration G is relatively small, the particles have to be either very dense or large to obtain sufficiently small λ. This is why GrFFF is most suited to the separation of larger particles in the steric mode (Giddings and Myers 1978). Sedimentation FFF (SdFFF) was introduced to obtain the increased centrifugal accelerations necessary for the retention and separation of smaller particles.

The retention ratio for steric mode FFF is given by

$$R = 6\gamma\alpha(1-\alpha) \tag{1.25}$$

in which α for a spherical particle of diameter d is equal to $d/(2w)$ and γ is an empirical correction factor of order unity that accounts for the influence of hydrodynamic lift forces and particle retardation effects close to the wall (Caldwell et al. 1979; Giddings et al. 1979; Williams et al. 1992, 1994, 1996b). Because of the unpredictability of γ, it is generally necessary to use some form of calibration in GrFFF. GrFFF remains a useful technique because of its affordability, its applicability to coarse inorganic and environmental materials, and its gentle treatment of materials such as biological cells. Even though the Earth's gravitational field cannot be altered, a programmed field strength may be obtained by gradually altering the orientation of the channel relative to the horizontal. The net transverse force on particles may also be programmed by continuously changing the carrier density or viscosity (Park et al. 2008) or by programming the carrier flow rate (Chmelík 1999; Plocková and Chmelík 2000, 2001, 2006; Plocková et al. 2002). Interestingly, GrFFF

was used for the first demonstration of the cyclical mode of FFF (Giddings 1986; Lee et al. 1988). In this mode of operation, particles are separated according to differences in their mobilities due to interaction with the alternating field.

1.5 Sedimentation Field-Flow Fractionation

Sedimentation FFF (SdFFF) in its conventional form was described in 1974 by Giddings, Yang, and Myers (Giddings et al. 1974). Berg and Purcell (1967) had previously demonstrated a form of SdFFF carried out within a film of fluid flowing down the inside of a spinning centrifuge with a vertical axis. This design was not as practical as the conventional form which uses a thin and relatively narrow channel wrapped around the inside of a centrifuge basket. Typically, channels are around 1–2 cm wide, 60–90 cm long, and have thicknesses of 125–250 μm. The radius of curvature of the channels is typically about 10 or 15 cm and these have maximum rotation rates of about 4900 or 2000 rpm, respectively. A prototype instrument having a radius of curvature of 9.9 cm with an upper rotation limit of 10,000 rpm has also been mentioned in the literature (Kato et al. 2019). The geometry of the system is illustrated in Figure 1.7. It has been shown by Martin (Martin 1996, 1997) that the curvature of the typical channels is sufficiently small that the fluid velocity profile does not deviate significantly from the parabolic profile of planar channels. The deviation of concentration profiles from exponential is also insignificant. Schure and Weeratunga (1991) also showed that the flow disturbance due to Coriolis forces in the thin spinning channel were expected to be small, but that for particles denser than the fluid it was better to flow the carrier fluid in the direction opposite to rotation where secondary flow tends to drive particles away from the side walls in the region close to the accumulation wall.

The retention and bandspreading equations derived for planar channels (Eqs. (1.2–1.6)) may therefore be used for SdFFF without significant error. The prediction of elution times and fractionating power may be made for various field decay programs (Giddings et al. 1987; Williams and Giddings 1987; Williams et al. 1987; Williams and Giddings 1994), which allows for the selection of optimum experimental conditions for given samples. It is also possible to transform fractograms obtained under arbitrary programmed conditions into particle size distributions using the integral method (Williams et al. 2001).

Particle–wall interaction may under certain conditions perturb the elution of submicron particles. There tends to be repulsion when the carrier fluid has a very low carrier ionic strength, for example. It has been found that the perturbation can be accounted for by the inclusion of a semiempirical parameter δ_w (having units of length) in the expression for R where the method of determining δ_w involves a relatively simple straight-line plot of retention data obtained at different field strengths (Williams et al. 1997). The δ_w parameter is effectively an adjustment to the steric exclusion distance; and depends on particle material, wall material, and carrier fluid composition; and is expected to be independent of particle size as well as field strength. Once determined, there is no reason why this correction cannot be

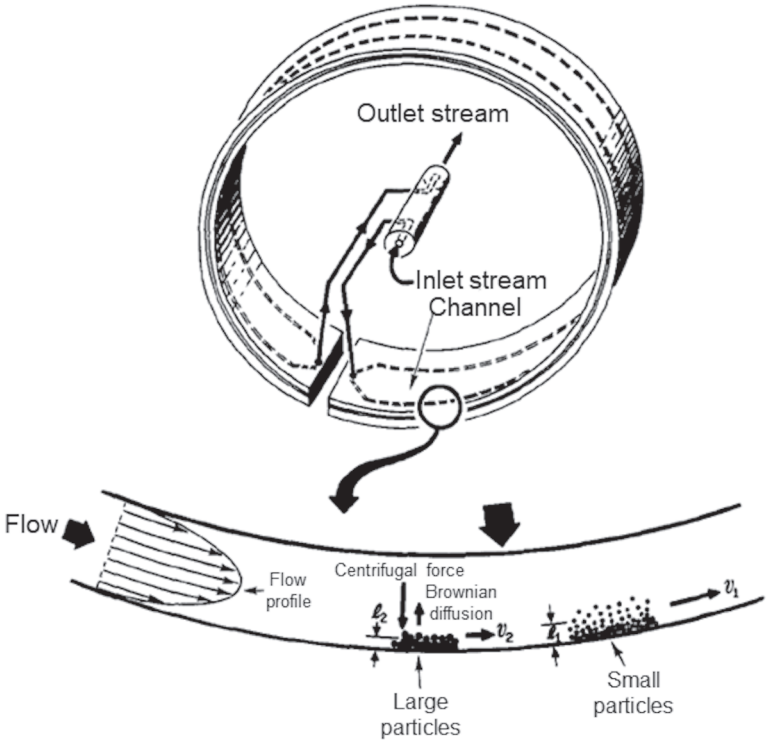

Figure 1.7 The upper figure shows a schematic of an SdFFF channel curved into a circular form to fit within a centrifuge basket. The fluid is carried to and from the channel *via* a rotating seal. The lower figure shows the mechanism of FFF separation of two components in the cross-section of a part of the curved channel. *Source*: Reprinted from Beckett et al. (1988) / with permission of ELSEVIER.

incorporated into the prediction of retention times and fractionating power under programmed conditions and into the integral method calculations for data analysis.

For the analysis of supramicron particles in the steric mode of elution, calibration with standards is of course necessary. This is because of the, still-not-well-understood, hydrodynamic lift forces and retardation effects close to the wall, as mentioned in relation to GrFFF (Caldwell et al. 1979; Williams et al. 1992, 1994, 1996b). There may be additional interactions with the channel wall, particularly at low carrier fluid ionic strength, that influence elution in the steric mode (Williams et al. 1996a). If the particle standards have the same composition as the unknown sample, then calibration can also account for these. If conditions are adjusted so that these composition effects are not significant, then the lift forces and hydrodynamic effects will depend on particle size and position and on carrier fluid velocity and viscosity only. In this case, the composition of the particle standards does not have to match that of the unknown sample. A difference in their density can be compensated by suitable adjustment of field strength so as to obtain equivalent sedimentation force for equivalent particle size (Giddings et al. 1991).

1.6 Thermal Field-Flow Fractionation

The separation of two polystyrene polymer standards in toluene by thermal FFF(ThFFF) was first demonstrated in 1967 using a relatively crude setup involving a Teflon capillary tube clamped between heated and cooled plates (Thompson et al. 1967). A better design using two 3- m-long, square cross-section, stainless steel chambers clamped around a Teflon gasket (to form the channel), one heated by passing hot oil through it and the other cooled by a flow of cold water, was described in 1969 (Thompson et al. 1969). The external chamber faces forming the channel walls were polished to a mirror finish. This planar channel was shown to give much better performance than the capillary, although separation of up to four polystyrene standards took around 50 hours, in spite of using a programmed decay of the temperature gradient. A design much closer to that of modern instruments was described in 1974 (Myers et al. 1974). This channel used a Mylar spacer clamped between two polished copper blocks, one heated electrically and the other cooled by an internal flow of cold water. The channel was just 35.6 cm long, 2.54 cm wide, with a Mylar spacer of thickness 0.0254 or 0.0127 cm. A second channel with gold-plated surfaces was used for aqueous carriers. The design has since been refined, but has not changed substantially. An exploded view of such a ThFFF channel is shown in Figure 1.8.

Today's instruments are constructed of highly polished, chrome- or nickel-plated copper alloy blocks with a Mylar spacer, from which the channel has been excised, clamped between them. The channels are typically 40–50 cm long, 1–2 cm wide, and a spacer of 127 μm or less in thickness is used. Holes through the heated block carry the sample and carrier fluid to the channel inlet and from the channel outlet to the detector. Electrical cartridge heaters are used to heat one of the blocks, while cold water circulates through the other. The temperature at the surfaces of the two blocks is constantly monitored, and the cartridge heaters cycled on and off under the control of a computer to maintain the required temperature gradient. As in other forms of FFF, a high-performance liquid chromatography (HPLC) pump is used to deliver the carrier fluid, an injection valve is used to introduce the sample

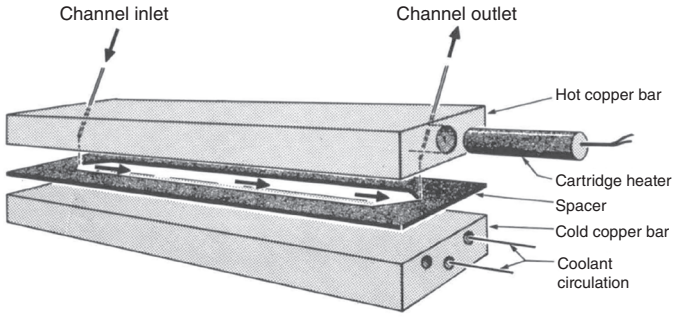

Figure 1.8 Exploded view of the main components of a ThFFF channel. *Source*: Giddings et al. (1990) / American Chemical Society.

(typically 20 µL), and one or more HPLC detectors are used to detect and possibly characterize the eluting species. Janča and coworkers have advocated the use of a smaller ThFFF channel, termed the microthermal FFF (Janča 2002b, 2002a; Janča et al. 2003; Janča 2008). These channels are typically 7.6 cm long, 3.2 mm wide, and have thicknesses of 100 µm, although thinner channels have also occasionally been used in conventional instruments. A reduced detector cell volume is necessary with the microthermal FFF channel, and the sample size is also reduced to just 1 µL.

ThFFF makes use of thermal diffusion to drive the sample species to the colder, accumulation wall. The transverse migration velocity is described by

$$|u| = D_T \frac{\mathrm{d}T}{\mathrm{d}x} \tag{1.26}$$

where D_T is the thermal diffusion coefficient and $\mathrm{d}T/\mathrm{d}x$ is the gradient in temperature. The value of D_T depends on the nature of both the sample species and the carrier fluid, and it also appears to have a dependence on temperature (Brimhall et al. 1985). Values of D_T have been found to be independent or nearly independent of polymer molecular weight (Schimpf and Giddings 1989), but this is not certain to be the case for colloids (Liu and Giddings 1992; Shiundu et al. 1995, 2003). The retention parameter is given approximately by

$$\lambda = \frac{D}{|u|\,w} = \frac{D}{D_T(\mathrm{d}T/\mathrm{d}x)w} \approx \frac{D}{D_T \Delta T} \tag{1.27}$$

where ΔT is the temperature drop across the channel thickness. If D_T is independent of molecular weight, λ is seen to vary with molecular diffusion coefficient D. Note that the ratio D_T/D is equivalent to α/T where α is the thermal diffusion factor.

The phenomenon of thermal diffusion is still poorly understood, and D_T values cannot be predicted (see, for example, Schimpf and Semenov (2000); Semenov and Schimpf (2020); Zheng (2002)). Besides being an analytical technique for determining the molecular weight distributions of polymers or size distributions of colloids, ThFFF is an excellent technique for determining D_T for different polymeric or colloidal materials in different fluid media and at different temperatures. For this purpose, it is necessary to model the retention in ThFFF to a high degree of accuracy. There are many features of ThFFF that contribute to small deviations from the classical FFF retention theory. The temperature gradient across the channel thickness is not quite constant, as assumed in the final form on the right-hand side of Eq. (1.27), due to the temperature dependence of the thermal conductivity of the solvent. The fluid viscosity varies across the channel thickness with the temperature, which influences the fluid velocity profile. The ratio of D/D_T is temperature dependent, so the concentration profile deviates from the classical exponential profile. The thermal expansion of the fluid with temperature across the channel thickness also influences the concentration profile slightly. Approximate corrections for all of these effects have been incorporated into the modeling of retention in ThFFF, and this allows for the extraction of D_T values from retention times of standards measured under known experimental conditions (see Giddings et al. (1976a); Gunderson et al. (1984); van Asten et al. (1994); Martin et al. (2002); Myers et al. (1974), for example).

The determination of molecular weight distributions of unknown samples generally requires calibration using narrow polymer standards. This is because D_T and D may be uncertain or unknown, and some of the system parameters may also be uncertain. In this case, it is sufficient to take care of only the major perturbations to retention and bandspreading and to have a consistent treatment of standards and unknown in order to determine the distribution of the sample. The aspect having the most effect on retention and bandspreading is the distortion of the velocity profile. Martin and Giddings (1981) showed how a small distortion to the parabolic velocity profile of classical FFF could be accounted for by a third-degree polynomial of the form

$$v(\xi) = 6\langle v\rangle[(1+\upsilon)\xi - (1+3\upsilon)\xi^2 + 2\upsilon\xi^3] \tag{1.28}$$

where ξ $(= x/w)$ is the fractional distance across the channel thickness measured from the accumulation wall, and υ is a correction term that is consistent with the limiting velocity gradient at the accumulation wall. The approach of Gunderson et al. (1984), which takes a known variation of fluid viscosity and thermal conductivity into account, results in a fifth-order expression in ξ for v. This may be approximated by the third-order expression of Eq. (1.28) by equating the slopes $\mathrm{d}v/\mathrm{d}\xi$ at the cold wall close to which the sample species are located during elution or simply equating the first-order coefficients. The solution for υ is thereby obtained for the assumed temperature dependencies of viscosity and thermal conductivity for any cold wall temperature T_c and temperature drop ΔT. Belgaied et al. (1994) generalized this approach to determining the solution for υ. They also carried out a convenient empirical fitting of υ to a function of T_c and ΔT for 12 different organic fluids.

If the concentration profiles are assumed not to deviate strongly from exponential, Martin and Giddings (1981) showed that for the third-order velocity profile of Eq. (1.28), the retention ratio is given by

$$R = 6\lambda\{\upsilon + (1 - 6\lambda\upsilon)[\coth(1/2\lambda) - 2\lambda]\} \tag{1.29}$$

The retention ratio for each standard is obtained from the measured elution time and is given by t^0/t_r, or $V^0/\dot{V}t_r$, and knowing υ, Eq. (1.29) may be solved for λ. Giddings (1994) proposed a universal calibration for ThFFF that may be written in the form

$$\frac{D}{D_T} = \phi_k\left(\frac{M}{10^k}\right)^{-n} \tag{1.30}$$

where D/D_T must be obtained from the extracted values of λ, and ϕ_k and n are best-fit parameters. This is useful only if T_c is held constant for both standards and the unknown sample. The approach was extended by Cao et al. (1999) to allow for variation of T_c. For the purposes of calibration, it is assumed that the ratio D/D_T is associated with temperature T_c rather than some temperature at the zone center of gravity, for example. This assumption simplifies the approach and does not introduce significant errors. It follows that

$$\left(\frac{D}{D_T}\right)_c = \lambda\theta_c\Delta T \tag{1.31}$$

where θ_c accounts for the small difference between the gradient in temperature at the cold wall $(\mathrm{d}T/\mathrm{d}x)_c$ and $\Delta T/w$ due to the variation of thermal conductivity with temperature

$$\left(\frac{\mathrm{d}T}{\mathrm{d}x}\right)_c = \left(1 + \frac{\mathrm{d}\kappa}{\mathrm{d}T}\frac{\Delta T}{2\kappa_c}\right)\frac{\Delta T}{w} = \theta_c\frac{\Delta T}{w} \tag{1.32}$$

in which κ_c is the thermal conductivity at T_c, and $\mathrm{d}\kappa/\mathrm{d}T$ is the rate of change of κ with T. If the standards are eluted at several different T_c, regression of the data may be carried out to an equation of the form

$$\lambda\theta_c\Delta T = \phi_{k,\,298}\left(\frac{T_c}{298.15}\right)^m\left(\frac{M}{10^k}\right)^{-n} \tag{1.33}$$

where an additional best-fit parameter m is obtained, as well as a temperature corrected $\phi_{k,\,298}$ rather than ϕ_k.

Once these three best-fit parameters, $\phi_{k,\,298}$, m and n, have been determined, it is possible to predict λ and hence elution time as a function of M for any flow rate $\dot{V}$, T_c, and ΔT. This can be done for isocratic (constant) conditions or even for programmed operations where any, or even all, of these parameters vary with time. The continuous monitoring of $\dot{V}$, T_c, and ΔT during the elution of an unknown sample would allow the transformation of the elution profile to a molecular weight distribution using the general integral method (Williams et al. 2001).

For the assumed third-order velocity profile of Eq. (1.28), the product of the nonequilibrium bandspreading parameter χ and retention ratio R is given by (Martin and Giddings 1981; Williams 2000a)

$$\begin{aligned}\chi R = 12\lambda^2\{&\left[-1 + 24\lambda^2 + 336\lambda^4 + 12(1 - 58\lambda^2 - 672\lambda^4)\lambda\nu\right.\\ &\left. - 24(1 - 216\lambda^2 - 2232\lambda^4)\lambda^2\nu^2\right]\\ &+ 6\lambda[1 - 20\lambda^2 - 8(1 - 69\lambda^2)\lambda\nu - 24(1 + 168\lambda^2)\lambda^2\nu^2]\ \coth(1/2\lambda)\\ &+ [1 - 12\lambda^2 - 12(1 - 18\lambda^2)\lambda\nu + 36(1 - 24\lambda^2)\lambda^2\nu^2]\coth^2(1/2\lambda)\\ &- 6\lambda[1 - 12\lambda\nu + 36\lambda^2\nu^2]\coth^3(1/2\lambda)\}\end{aligned} \tag{1.34}$$

and for conditions corresponding to significant retention where coth $(1/2\lambda)$ approaches unity, Eq. (1.34) reduces to

$$\begin{aligned}\chi R = 144\lambda^4&\left[1 - 10\lambda + 28\lambda^2 + (2 - 40\lambda + 276\lambda^2 - 672\lambda^3)\upsilon\right.\\ &\left. + (1 - 30\lambda + 360\lambda^2 - 2016\lambda^3 + 4464\lambda^4)\upsilon^2\right]\end{aligned} \tag{1.35}$$

The use of these equations allows the calculation of molecular-weight-based fractionating power F_M as a function of M for any programmed conditions (Williams et al. 2001). The importance of F_M as an indicator of the quality of the fractionation has been explained in terms of the residual polydispersity of the eluting species in the channel outlet stream (Williams 2016). It has already been pointed out that polydispersity can influence the accuracy of information returned by multi-angle light scattering detection, for example, and that conditions should be optimized to obtain an acceptable level of fractionating power across the full range of a polydisperse sample.

1.7 Electrical Field-Flow Fractionation

To separate charged species by electrical FFF (ElFFF), a potential gradient must be maintained across the channel thickness. Positively or negatively charged species are then driven toward one wall or the other as they are carried by the flow along the channel. ElFFF was first demonstrated by Giddings and coworkers (Caldwell et al. 1972; Giddings et al. 1976b; Kesner et al. 1976). These early instruments used a semipermeable membrane channel with electrodes mounted in chambers external to the channel, and the electrodes were from 1.7 to 5.1 cm apart. Buffer was driven continuously through the chambers to remove the gases produced by electrolysis. It was realized that the voltage drop across the channel thickness was a small fraction of that between the electrodes. Not only is the channel thickness a small fraction of the distance between the electrodes, but there was some electrical resistance due to the membrane walls and a greater resistance across the porous support plates, if present. It was calculated that the potential gradient across the channel could be as low as 0.3% of the potential gradient between electrodes when electrode spacing was 2.44 cm and channel thickness was 356 μm, and cellulose acetate membranes of 12 kDa cutoff, forming the channel walls, were cast onto two 0.318-cm-thick polyethylene support plates with 100-μm pores. There was more electrical resistance due to the porous support plates than the membranes, but without them, the channel thickness could not be made consistently uniform. Lightfoot and coworkers proposed an alternative approach where a hollow fiber was subjected to a transverse potential gradient; this they termed hollow fiber electropolarization chromatography (Chiang et al. 1979; Lightfoot et al. 1981; Reis and Lightfoot 1976; Reis et al. 1978; Shah et al. 1979). It would have suffered from the same problem of low potential gradient in the channel as the previous parallel wall channels, and furthermore, tubular channel geometry with transverse field is not ideal for implementing FFF (Giddings 2000). An annular channel design was also described in which concentric porous glass tubes served as channel walls (Davis et al. 1987). This device did not perform as well as expected.

In 1993, Caldwell and Gao (1993) proposed a new approach to parallel wall ElFFF. In this design, the channel walls themselves served as the electrodes. These were smooth graphite plates separated by a Mylar spacer. Such a design is shown in exploded form in Figure 1.9. A potential difference of up to 2 V could be applied to the thin (178 μm) channel without electrolytic breakdown of the aqueous carrier solution. This resulted in a higher potential gradient across the channel than had been possible with earlier designs. However, it was apparent that the voltage drop across the channel was far lower than the voltage drop applied to the graphite plates. This was due to electrical polarization layers at the electrode surfaces. The ionic strength of the carrier solution has an influence on the polarization, of course, but it is often not possible to significantly reduce ionic strength when biological species are to be fractionated. The system was later shown to be effective at fractionating polystyrene latex particles in both normal and steric modes using a low ionic strength carrier solution (Tri et al. 2000).

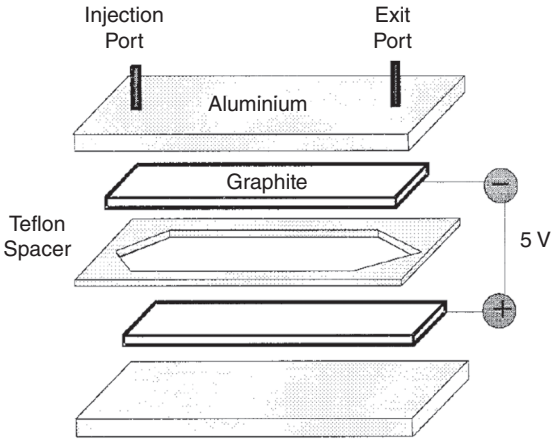

Figure 1.9 Exploded view of the main components of an ElFFF channel. *Source*: Tri et al. (2000) / American Chemical Society.

The retention parameter in ElFFF is given by

$$\lambda = \frac{D}{\mu_e E_{\text{eff}} w} = \frac{kT}{3\pi\eta d_h \mu_e E_{\text{eff}} w} \tag{1.36}$$

where μ_e is the particle electrophoretic mobility and E_{eff} is the effective electric field (potential gradient), and it was noted that the particle hydrodynamic diameter includes the double layer thickness which is significant at low ionic strength.

Palkar and Schure (1997a) studied the time dependence of the electrode polarization effect as well as the influence of flow rate. They also studied the influence of sample size on retention and the effect of sample conductivity (Palkar and Schure 1997b). It is clear that the precise prediction of retention times in ElFFF is not a simple matter.

Micro-machined ElFFF channels were introduced in 1998 by Gale et al. (1998). The channels were 4–6 cm long, just 20–30 μm thick, and 0.4–8 mm broad. Titanium followed by gold was sputtered onto the silicon wafer and glass plate walls to serve as electrodes (titanium was used for its good adhesion to silicon). Sample volumes were typically as small as 0.1 μL, injected through a septum close to the channel inlet. The advantages of miniaturization of ElFFF were later examined in theory and practice (Gale et al. 2001, 2002). The advantages lie in improved efficiency, faster sample relaxation, reduced steric inversion diameter, and reduced system time constant (the time for the system to stabilize on applying the potential gradient). The reduced time constant opened up the possibility of using alternating electric fields for cyclical operation. The electrode polarization problem could then be circumvented using a square-wave, cyclical electric field with optimized frequency (Lao et al. 2002; Gale and Srinivas 2005). In cyclical operation, species are separated according to differences in their electrophoretic mobilities μ_e, rather than in the ratios of D/μ_e. It is the mobility and the frequency of the cycling field that determines the fraction of time spent in the faster-flowing regions as compared to the regions close to the walls (Giddings 1986; Lee et al. 1988; Stevens 1990). Cyclical ElFFF

has been shown to be an effective separation technique for submicron-charged particles. Improvements to modeling (Chen and Chauhan 2007; Kantak et al. 2006), experimental optimization (Gigault et al. 2011; Srinivas et al. 2010), and the advantage of operation with biased fields (Ornthai et al. 2015; Tasci et al. 2013) have yielded significant improvements.

1.8 Magnetic Field-Flow Fractionation

Different approaches to implementing magnetic FFF (MgFFF) have been considered through the years. Many of the early efforts were reviewed by Carpino et al. (2005b). Studies involving simple capillary tubes with transverse applied magnetic field gradients were reported by Mori (1986), Latham et al. (2005), and Vickrey and Garcia-Ramirez (1980). Tubular channel geometry with a transverse applied field is not well suited to the implementation of FFF (Giddings 2000), and the field gradients were relatively small. Mori (1986) demonstrated only slight retention of Ni^{2+} protein complexes, and Latham et al. (2005) obtained separation of 13-nm $CoFe_2O_4$ particles in hexane from 6-nm Fe_2O_3 particles that eluted with the void peak. Nomizu et al. (2001) used an intermittent transverse magnetic gradient, provided by an electromagnet, applied to a capillary tube to show separation between retained 0.6-μm magnetite particles from effectively non-retained 0.7-μm hematite particles in an aqueous carrier with 0.1% sodium oleate as a dispersive agent. It is not possible to determine whether retention of magnetite particles was in accord with magnetophoretic mobility as would be expected for the cyclical FFF mechanism, or whether it was simply a function of the time captured during periods of applied transverse field gradient.

Fukui, Ohara, and coworkers (Fukui et al. 2008, 2009; Takahashi et al. 2006) proposed the use of high-temperature superconducting magnets to obtain higher field gradients of 200 T/m or more. They carried out theoretical modeling of separation in capillaries subjected to such field gradients. They did not allow for relaxation to steady-state distributions before elution, however, and their simulations reflected separation due to differences in relaxation across the capillary cross-section. Therefore, the mechanism considered was not strictly that of FFF.

In 1984, Schunk, Gorse, and Burke (Gorse et al. 1984; Schunk et al. 1984) reported the use of a parallel-plate channel with a transverse field gradient generated by an electromagnet. They were able to separate singlet 0.8-μm-rod-shaped iron oxide particles used in the recording industry from doublets. Again, the field gradient was rather small. As a means of creating high field gradients in a channel, Semenov and Kuznetsov (1986) proposed mounting a ferromagnetic wire at the axis of a tubular channel and magnetizing the wire with an external magnetic field. The concept is taken from high-gradient magnetic separation (HGMS) technology (Oberteuffer 1973) widely used nowadays for immunomagnetic cell separation. The small surface of the wire would serve as the accumulation wall, which would make the system susceptible to overloading. The field gradient would also tend to increase

rapidly with an approach to the wire which would tend to capture species which is the objective in HGMS. Semenov (1986) solved these problems by proposing that a uniform array of wires be embedded in one of the walls of a parallel-plate channel. The regular spacing of the wires was predicted to generate a fairly uniform field gradient in the channel. There have since been several modeling efforts and simulations of particle separations for such a design (Karki et al. 2001; Ohara et al. 1996; Ohara 1997; Ohara et al. 2000; Tsukamoto et al. 1995; Wang et al. 1997) and just one experimental implementation where there was shown to be slight retention of some transition metal salts (Mitsuhashi et al. 2002).

The most successful approach to MgFFF to date uses a quadrupole electromagnet and helical channel (Carpino et al. 2005a, 2005b, 2007; Williams 2012; Williams et al., 2009b, 2010c). A relatively small aperture (1–2 cm diameter) quadrupole electromagnet can generate uniform field gradients comparable to those found in the much bigger (10 cm diameter) superconducting quadrupoles (Takahashi et al. 2006), and these can be efficiently exploited using a helical channel mounted axisymmetrically to the field, close to the pole pieces. The helical channel has the advantage over a simple annular channel in that it is far simpler to maintain uniform thickness. It is also much easier to introduce fluid uniformly to the helical channel than to a full annular channel, and this is also true for the withdrawal of the fluid at the channel outlet. Also, the helical flow path carries all sample components through any small variations in field gradient around the annular space that would contribute to bandspreading in an annular channel. The use of an electromagnet also allows for very easy implementation of programmed decay of magnetic field gradient during sample analysis (Williams et al. 2010a). The quadrupole electromagnet and spiral channel are shown schematically in Figure 1.10 a and b, respectively, and a photograph of the system in Figure 1.10 c.

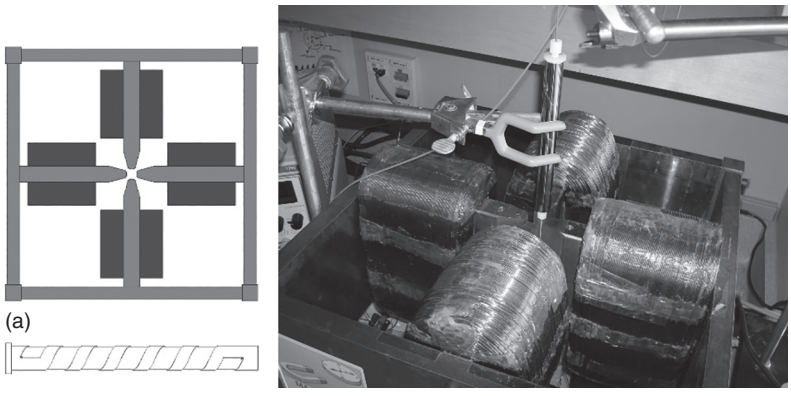

Figure 1.10 (a) Schematic of the cross-section of the soft iron pole pieces and yoke (pale gray) and electrical coils (dark gray); (b) Schematic of spiral channel machined into Delrin™ (DuPont) rod that fits tightly into a stainless steel cylinder; *Source*: Carpino et al. (2005b) / with permission of ELSEVIER. (c) Photograph of the MgFFF system with the assembled spiral channel ready for an introduction to the quadrupole aperture.

The small deviations from parabolic of longitudinal and azimuthal velocity profiles in annular flow have been studied, as well as their influence on the retention ratio in a helical channel (Williams et al. 2009a, 2010b). However, if the channel thickness is relatively small compared to its radius of curvature, then the retention ratio and nonequilibrium bandspreading parameter are well approximated by the classical model equations (see Eqs. (1.2–1.6)).

The force F_m experienced by a magnetic particle in suspension placed in a magnetic field gradient is given by

$$F_m = V_m \Delta\chi \frac{B}{\mu_0} \nabla B = V_m M \nabla B \tag{1.37}$$

where V_m is the volume of magnetizable material contained in the particle, $\Delta\chi$ is the difference in magnetic susceptibility between the magnetizable material and the other materials present (the fluid and the other particle components, all assumed to have small susceptibility), μ_0 is the magnetic permeability of free space, M is the magnetization of the magnetizable material in the particles at the applied magnetic field B (other materials assumed to have negligible magnetization), and ∇B is the gradient in the magnitude of the magnetic field across the channel thickness. In an ideal quadrupole, the magnitude of the magnetic field B increases linearly with distance from the axis

$$B = \frac{r}{r_o} B_o \tag{1.38}$$

where r is the distance from the axis, r_o is the radius of the channel outer wall, and B_o is the magnitude of the field at r_o. The field gradient ∇B across the channel thickness is therefore constant and equal to B_o/r_o. Replacing F_G in Eq. (1.24) by F_m, the retention parameter λ is given by

$$\lambda = \frac{kT}{F_m w} = \frac{kT\, r_o}{V_m M B_o w} \tag{1.39}$$

The magnetization is a function of local field B as may be seen in Eq. (1.37), where $M = \chi B/\mu_0$, and for paramagnetic and diamagnetic materials, χ is constant. However, particles that are of particular interest for magnetic characterization are the superparamagnetic nanoparticles used for immunomagnetic labeling of specific biological cell types or used as drug carriers for magnetically targeted cancer treatment. These are composite particles where the iron oxide nanoparticles are coated with a biocompatible material such as dextran and which also may carry a chemotherapeutic drug and/or antibodies to a specific cell type. The magnetization M of the superparamagnetic component does not increase indefinitely with B. It approaches a saturation magnetization M_s at relatively low fields of 0.1–0.2 T. In this case, the concentration profile approaches an exponential, with λ given by Eq. (1.39) with $M = M_s$. Even at low field strength, where the magnetic material is approximately paramagnetic, the concentration profile does not deviate significantly from an exponential in the thin channels used.

For the characterization of superparamagnetic nanoparticles, it is not necessary for them to remain magnetically saturated during elution. If the full magnetization

curve (M as a function of B from zero to saturation) is known for the magnetic material included in a sample of magnetic nanoparticles, then it is possible to predict retention times as a function of V_m, or the equivalent spherical diameter d_m, for any applied field or programmed field decay. There is one caveat. Although only the magnetic component responds to the field gradient, the steric exclusion correction, if it is considered, is dependent on the overall particle size. They do tend to be rather small (less than about 200 nm), however, and the steric correction will be correspondingly small. Using the general integral approach developed for data reduction (Williams et al. 2001), it is also possible to transform an elution profile into a distribution in V_m or d_m. Regarding the prediction of fractionating power, nonequilibrium bandspreading is a function of D and therefore of overall particle size (see Eq. (1.4) for the contribution to plate height). It would be necessary to make some assumptions concerning particle size. For example, particles may be assumed to have similar sizes (determined by light scattering or AsFlFFF, perhaps) but contain differing amounts of magnetic components.

It should be pointed out that MgFFF applies to the fractionation of superparamagnetic nanoparticles only if they have a nonmagnetic coating. Without the coating, the magnetic interaction between the magnetized particles causes aggregation, and fractionation is not possible (Williams et al. 2010c).

1.9 Novel Techniques

1.9.1 Combined Fields

The combination of more than a single transverse field can sometimes be advantageous. Various combinations have been explored. Chen et al. (1988) showed that a steric (or hyperlayer) separation of supramicron polystyrene particle standards by symmetrical FlFFF could be improved if gravity was imposed in the same direction as the cross-flow. They called the technique gravity-augmented FlFFF.

Liu and Giddings (1991) reported the use of thermal-electrical FFF for the separation of submicron polystyrene particle standards in acetonitrile. The retention of the particles due to the thermal gradient could be enhanced or reduced by the application of a voltage gradient across the channel.

Ultrasound-gravitational FFF has been described (Yin et al., 2013) in which the force due to a resonant acoustic field on microparticles toward the node at the channel midpoint is opposed by gravity. No experimental results were presented, but particles of different compositions were expected to be driven to different equilibrium positions across the channel thickness and be carried to the outlet at different times. The technique would not have the capability to separate particles by size alone because forces due to both the standing acoustic wave and gravity depend on particle volume.

Johann et al. (2015) constructed an AsFlFFF instrument in which an electrical field can be applied across the channel thickness. They were able to determine electrophoretic mobilities of nanoparticles and proteins by measuring elution

times using cross-flow alone and then measuring the increase in elution times with the application of a voltage gradient. They were also able to show enhanced separation with the application of the electrical field. Further studies have been reported recently following the commercializing of this electrical AsFlFFF system (also referred to as EAF4) (Choi et al. 2020; Metzger et al. 2021; Kohl et al. 2021).

The technique of dielectrophoretic FFF (DEP-FFF) requires the opposition of dielectrical force and gravity (Huang et al. 1997; Markx et al. 1997; Wang et al. 1998, 2000; Yang et al. 2000). A negative dielectrophoretic force on microparticles drives them away from an array of microelectrodes in the lower channel wall, and this is opposed by gravity if they are denser than the fluid. The dielectrophoretic force varies strongly with distance from the electrodes, while gravity exerts a constant force. Both forces vary with the volume of the particles. The equilibrium position and elution time depend on both the density and the polarizability of the particle. The technique has been found to separate various types of biological cells based on differences in their polarizability.

An interesting technique proposed by Janča and Audebert combines an electrical field with gravity to implement a type of hyperlayer FFF based on isopycnic focusing (Janča and Audebert 1993, 1994). A colloidal density modifier, such as Percoll, is added to the carrier fluid. This is driven by the electrical field to form a density gradient across the channel thickness, and the microparticles to be separated find their isopycnic equilibrium positions within this gradient under the influence of gravity. They were able to show the influence of voltage gradient on the retention ratios of different particles.

1.9.2 Two-Dimensional, Continuous Fractionation

There has been some development of two-dimensional FFF instruments for continuous fractionations. Giddings discussed the theoretical aspects of continuous FFF separations (Giddings 1984, 1990b). It was explained that a selective FFF separation in one direction can be combined with a field-induced migration at right angles resulting in different trajectories to different collection points for different species. The field-induced migration may or may not be selective, but if it is selective, its selectivity must differ from that of the FFF separation. The migration at right angles to the FFF separation may also be provided by a non-selective flow or bulk displacement.

A continuous steric FFF device was developed that used a planar channel whose breadth was set at an angle to the horizontal so that particles sedimented across the channel breadth as they migrated in steric mode along the channel length in the horizontal direction (Myers and Giddings 1979; Schure et al. 1985). Particles of different sizes could be collected at different outlets along the lower edge of the channel. Ivory et al. (1995) constructed a continuous SdFFF instrument that used a centrifuge rotor housing a channel with a conic cross-section. The channel was therefore at an angle to the radius. It was intended that the migration in the direction of flow and rotation was to be *via* the mechanism of normal or steric mode SdFFF and the migration across the channel breadth by sedimentation. Unfortunately, separation appeared to be disrupted by flow instabilities in the rotating channel.

Pearlstein and Shiue (1995) presented a concept for continuous FFF separation in the annular space between concentric cylinders, one of which rotates while the other is held stationary. The carrier fluid flows axially within the annulus and the sample is introduced at a fixed point on the circumference at the channel inlet. Sample species were predicted to follow different spiral paths along the annular channel to be collected at different points around the circumference of the outlet. They presented only a mathematical model of the expected separation for such a system.

Vastamäki and coworkers (Vastamäki et al. 2014, 2001, 2003, 2005) have developed a continuous two-dimensional ThFFF instrument. It makes use of radial carrier fluid flow between two circular plates, the upper of which is stationary and heated, while the lower is slowly rotated and is cooled. The carrier fluid is introduced at the center of the upper heated disk, and the sample is continuously fed into a second inlet that is a small distance from the axis of the upper disk. Sample species relax to the lower rotating disk and migrate radially outward by the mechanism of ThFFF. At the same time, they are angularly displaced by the rotation of the lower disk. Different species follow different curved paths to the circumference where they are collected at several collection ports around the edges of the disks.

There are numerous potentially useful combinations of fields, flows, as well as field and flow directions that may be exploited for separations of different species of differing size or composition. There are likely to be many interesting developments in the future.

References

Ahn, J.Y., Kim, K.H., Lee, J.Y. et al. (2010). Effect of asymmetrical flow field-flow fractionation channel geometry on separation efficiency. *Journal of Chromatography A* 1217 (24): 3876–3880. https://doi.org/10.1016/j.chroma.2010.04.021.

Beckett, R., Nicholson, G., Hart, B.T. et al. (1988). Separation and size characterization of colloidal particles in river water by sedimentation field-flow fractionation. *Water Research* 22 (12): 1535–1545. https://doi.org/10.1016/0043-1354(88)90166-2.

Beckett, R., Sharma, R., Andric, G. et al. (2007). Illustrating some principles of separation science through gravitational field-flow fractionation. *Journal of Chemical Education* 84 (12): 1955–1962. https://doi.org/10.1021/ed084p1955.

Belgaied, J.E., Hoyos, M., and Martin, M. (1994). Velocity profiles in thermal field-flow fractionation. *Journal of Chromatography A* 678 (1): 85–96. https://doi.org/10.1016/0021-9673(94)87077-2.

Berg, H.C. and Purcell, E.M. (1967). A method for separating according to mass a mixture of macromolecules or small particles suspended in a fluid, III. Experiments in a centrifugal field. *Proceedings of the National Academy of Sciences* 58 (5): 1821–1828. https://doi.org/10.1073/pnas.58.5.1821.

Berg, H.C., Purcell, E.M., and Stewart, W.W. (1967). A method for separating according to mass a mixture of macromolecules or small particles suspended in a fluid, II. Experiments in a gravitational field. *Proceedings of the National Academy of Sciences* 58 (4): 1286–1291. https://doi.org/10.1073/pnas.58.4.1286.

Brimhall, S.L., Myers, M.N., Caldwell, K.D., and Giddings, J.C. (1985). Study of temperature dependence of thermal diffusion in polystyrene/ethylbenzene by thermal field-flow fractionation. *Journal of Polymer Science Polymer Physics Edition* 23 (12): 2443–2456. https://doi.org/10.1002/pol.1985.180231203.

Caldwell, K.D., Kesner, L.F., Myers, M.N., and Giddings, J.C. (1972). Electrical field-flow fractionation of proteins. *Science* 176 (4032): 296–298. https://doi.org/10.1126/science.176.4032.296.

Caldwell, K.D., Nguyen, T.T., Myers, M.N., and Giddings, J.C. (1979). Observations on anomalous retention in steric field-flow fractionation. *Separation Science and Technology* 14 (10): 935–946. https://doi.org/10.1080/01496397908058103.

Caldwell, K.D. and Gao, Y.-S. (1993). Electrical field-flow fractionation in particle separation. 1. Monodisperse standards. *Analytical Chemistry* 65 (13): 1764–1772. https://doi.org/10.1021/ac00061a021.

Cao, W., Williams, P.S., Myers, M.N., and Giddings, J.C. (1999). Thermal field-flow fractionation universal calibration: extension for consideration of variation of cold wall temperature. *Analytical Chemistry* 71 (8): 1597–1608. https://doi.org/10.1021/ac981094m.

Carlshaf, A. and Jönsson, J.Å. (1993). Properties of hollow fibers used for flow field-flow fractionation. *Separation Science and Technology* 28 (4): 1031–1042. https://doi.org/10.1080/01496399308029236.

Carpino, F., Moore, L.R., Chalmers, J.J. et al. (2005a). Quadrupole magnetic field-flow fractionation for the analysis of magnetic nanoparticles. *Journal of Physics: Conference Series* 17: 174–180. https://doi.org/10.1088/1742-6596/17/1/024.

Carpino, F., Moore, L.R., Zborowski, M. et al. (2005b). Analysis of magnetic nanoparticles using quadrupole magnetic field-flow fractionation. *Journal of Magnetism and Magnetic Materials* 293 (1): 546–552. https://doi.org/10.1016/j.jmmm.2005.01.071.

Carpino, F., Zborowski, M., and Williams, P.S. (2007). Quadrupole magnetic field-flow fractionation: a novel technique for the characterization of magnetic nanoparticles. *Journal of Magnetism and Magnetic Materials* 311 (1): 383–387. https://doi.org/10.1016/j.jmmm.2006.11.162.

Chen, X., Wahlund, K.-G., and Giddings, J.C. (1988). Gravity-augmented high-speed flow/steric field-flow fractionation: simultaneous use of two fields. *Analytical Chemistry* 60 (4): 362–364. https://doi.org/10.1021/ac00155a019.

Chen, Z. and Chauhan, A. (2007). Electrochemical response and separation in cyclic electric field-flow fractionation. *Electrophoresis* 28 (5): 724–739. https://doi.org/10.1002/elps.200600324.

Chiang, A.S., Kmiotek, E.H., Langan, S.M. et al. (1979). Preliminary experimental survey of hollow-fiber electro-polarization chromatography (electrical field-flow fractionation) for protein fractionation. *Separation Science and Technology* 14 (6): 453–474. https://doi.org/10.1080/01496397908068470.

Chmelík, J. (1999). Different elution modes and field programming in gravitational field-flow fractionation. I. A theoretical approach. *Journal of Chromatography A* 845 (1–2): 285–291. https://doi.org/10.1016/S0021-9673(99)00131-4.

Choi, J., Fuentes, C., Fransson, J. et al. (2020). Separation and zeta-potential determination of proteins and their oligomers using electrical asymmetrical flow field-flow fractionation (EAF4). *Journal of Chromatography A* 461625: https://doi.org/10.1016/j.chroma.2020.461625.

Davis, J.M., Fan, F.-R.F., and Bard, A.J. (1987). Retention by electrical field-flow fractionation of anions in a new apparatus with annular porous glass channels. *Analytical Chemistry* 59 (9): 1339–1348. https://doi.org/10.1021/ac00136a017.

Doshi, M.R., Gill, W.N., and Subramanian, R.S. (1975). Unsteady reverse osmosis or ultrafiltration in a tube. *Chemical Engineering Science* 30 (12): 1467–1476. https://doi.org/10.1016/0009-2509(75)85024-X.

Fuentes, C., Choi, J., Zielke, C. et al. (2019). Comparison between conventional and frit-inlet channel in separation of biopolymers by asymmetric flow field-flow fractionation. *Analyst* 144 (15): 4559–4568. https://doi.org/10.1039/C9AN00466A.

Fukui, S., Shoji, Y., Abe, R. et al. (2008). Numerical simulation of flow fractionation characteristics of magnetic chromatography using an HTS bulk magnet. *IEEE Transactions on Applied Superconductivity* 18 (2): 828–831. https://doi.org/10.1109/TASC.2008.921248.

Fukui, S., Shoji, Y., Ogawa, J. et al. (2009). Study of flow fractionation characteristics of magnetic chromatography utilizing high-temperature superconducting bulk magnet. *Science and Technology of Advanced Materials* 10 (1): 014610. https://doi.org/10.1088/1468-6996/10/1/014610.

Gale, B.K., Caldwell, K.D., and Frazier, A.B. (1998). A micromachined electrical field-flow fractionation (μ-EFFF) system. *IEEE Transactions on Biomedical Engineering* 45 (12): 1459–1469. https://doi.org/10.1109/10.730439.

Gale, B.K., Caldwell, K.D., and Frazier, A.B. (2001). Geometric scaling effects in electrical field flow fractionation. 1. Theoretical analysis. *Analytical Chemistry* 73 (10): 2345–2352. https://doi.org/10.1021/ac001463q.

Gale, B.K., Caldwell, K.D., and Frazier, A.B. (2002). Geometric scaling effects in electrical field flow fractionation. 2. Experimental results. *Analytical Chemistry* 74 (5): 1024–1030. https://doi.org/10.1021/ac015623p.

Gale, B.K. and Srinivas, M. (2005). Cyclical electrical field flow fractionation. *Electrophoresis* 26 (9): 1623–1632. https://doi.org/10.1002/elps.200410296.

Giddings, J.C. (1968). Nonequilibrium theory of field-flow fractionation. *Journal of Chemical Physics* 49 (1): 81–85. https://doi.org/10.1063/1.1669863.

Giddings, J.C., Yang, F.J.F., and Myers, M.N. (1974). Sedimentation field-flow fractionation. *Analytical Chemistry* 46 (13): 1917–1924. https://doi.org/10.1021/ac60349a046.

Giddings, J.C., Yoon, Y.H., Caldwell, K.D. et al. (1975). Nonequilibrium plate height for field-flow fractionation in ideal parallel plate columns. *Separation Science* 10 (4): 447–460. https://doi.org/10.1080/00372367508058032.

Giddings, J.C., Caldwell, K.D., and Myers, M.N. (1976a). Thermal diffusion of polystyrene in eight solvents by an improved thermal field-flow fractionation methodology. *Macromolecules* 9 (1): 106–112. https://doi.org/10.1021/ma60049a021.

Giddings, J.C., Lin, G.-C., and Myers, M.N. (1976b). Electrical field-flow fractionation in a rigid membrane channel. *Separation Science* 11 (6): 553–568. https://doi.org/10.1080/01496397608085344.

Giddings, J.C., Yang, F.J., and Myers, M.N. (1976c). Theoretical and experimental characterization of flow field-flow fractionation. *Analytical Chemistry* 48 (8): 1126–1132. https://doi.org/10.1021/ac50002a016.

Giddings, J.C., Yang, F.J.F., and Myers, M.N. (1976d). Flow field-flow fractionation: a versatile new separation method. *Science* 193 (4259): 1244–1245. https://doi.org/10.1126/science.959835.

Giddings, J.C. (1978). Displacement and dispersion of particles of finite size in flow channels with lateral forces. Field-flow fractionation and hydrodynamic chromatography. *Separation Science and Technology* 13 (3): 241–254. https://doi.org/10.1080/01496397808060222.

Giddings, J.C. and Myers, M.N. (1978). Steric field-flow fractionation: a new method for separating 1 to 100 μm particles. *Separation Science and Technology* 13 (8): 637–645. https://doi.org/10.1080/01496397808057119.

Giddings, J.C. (1979). ERRATA. Displacement and dispersion of particles of finite size in flow channels with lateral forces. Field-flow fractionation and hydrodynamic chromatography. *Separation Science and Technology* 14 (9): 869–870. https://doi.org/10.1080/01496397908060246.

Giddings, J.C., Myers, M.N., Caldwell, K.D., and Pav, J.W. (1979). Steric field-flow fractionation as a tool for the size characterization of chromatographic supports. *Journal of Chromatography* 185: 261–271. https://doi.org/10.1016/S0021-9673(00)85608-3.

Giddings, J.C. (1984). Two-dimensional separations: concept and promise. *Analytical Chemistry* 56 (12): 1258A–1264A. https://doi.org/10.1021/ac00276a003.

Giddings, J.C. (1985). Optimized field-flow fractionation system based on dual stream splitters. *Analytical Chemistry* 57 (4): 945–947. https://doi.org/10.1021/ac00281a037.

Giddings, J.C. (1986). Cyclical field field-flow fractionation: a new method based on transport rates. *Analytical Chemistry* 58 (9): 2052–2056. https://doi.org/10.1021/ac00122a027.

Giddings, J.C., Williams, P.S., and Beckett, R. (1987). Fractionating power in programmed field-flow fractionation: exponential sedimentation field decay. *Analytical Chemistry* 59 (1): 28–37. https://doi.org/10.1021/ac00128a007.

Giddings, J.C. (1990a). Hydrodynamic relaxation and sample concentration in field-flow fractionation using permeable wall elements. *Analytical Chemistry* 62 (21): 2306–2312. https://doi.org/10.1021/ac00220a010.

Giddings, J.C. (1990b). Two-dimensional field-flow fractionation. *Journal of Chromatography* 504: 247–258. https://doi.org/10.1016/S0021-9673(01)89530-3.

Giddings, J.C., Kumar, V., Williams, P.S., and Myers, M.N. (1990). Polymer separation by thermal field-flow fractionation: high-speed power programming. In: *Polymer Characterization: Physical, Spectroscopic, and Chromatographic Methods*, vol. 227, Ch. 1 (ed. C.D. Craver and T. Provder), 3–21. Washington, DC: American Chemical Society https://doi.org/10.1021/ba-1990-0227.ch001.

Giddings, J.C., Moon, M.H., Williams, P.S., and Myers, M.N. (1991). Particle size distribution by sedimentation/steric field-flow fractionation: development of a calibration procedure based on density compensation. *Analytical Chemistry* 63 (14): 1366–1372. https://doi.org/10.1021/ac00014a006.

Giddings, J.C. (1994). Universal calibration in size exclusion chromatography and thermal field-flow fractionation. *Analytical Chemistry* 66 (17): 2783–2787. https://doi.org/10.1021/ac00089a029.

Giddings, J.C. (2000). The field-flow fractionation family: underlying principles. In: *Field-Flow Fractionation Handbook*, vol. Ch. 1 (ed. M.E. Schimpf, K. Caldwell, and J.C. Giddings), 3–30. New York, NY: Wiley.

Gigault, J., Gale, B.K., Le Hecho, I., and Lespes, G. (2011). Nanoparticle characterization by cyclical electrical field-flow fractionation. *Analytical Chemistry* 83 (17): 6565–6572. https://doi.org/10.1021/ac2008948.

Gopalakrishnan, A., Bouby, M., and Schäfer, A.I. (2023). Membrane-organic solute interactions in asymmetric flow field flow fractionation: interplay of hydrodynamic and electrostatic forces. *Science of the Total Environment* 855: 158891. https://doi.org/10.1016/j.scitotenv.2022.158891.

Gorse, J., Schunk, T.C., and Burke, M.F. (1984). The study of liquid suspensions of iron oxide particles with a magnetic field-flow fractionation device. *Separation Science and Technology* 19 (13–15): 1073–1085. https://doi.org/10.1080/01496398408058349.

Granger, J., Dodds, J., Leclerc, D., and Midoux, N. (1986). Flow and diffusion of particles in a channel with one porous wall: polarization chromatography. *Chemical Engineering Science* 41 (12): 3119–3128. https://doi.org/10.1016/0009-2509(86)85049-7.

Gunderson, J.J., Caldwell, K.D., and Giddings, J.C. (1984). Influence of temperature gradients on velocity profiles and separation parameters in thermal field-flow fractionation. *Separation Science and Technology* 19 (10): 667–683. https://doi.org/10.1080/01496398408060668.

Hansen, M.E. and Giddings, J.C. (1989). Retention perturbations due to particle-wall interactions in sedimentation field-flow fractionation. *Analytical Chemistry* 61 (8): 811–819. https://doi.org/10.1021/ac00183a006.

Hansen, M.E., Giddings, J.C., and Beckett, R. (1989). Colloid characterization by sedimentation field-flow fractionation. VI. Perturbations due to overloading and electrostatic repulsion. *Journal of Colloid and Interface Science* 132 (2): 300–312. https://doi.org/10.1016/0021-9797(89)90245-2.

Huang, Y., Wang, X.-B., Becker, F.F., and Gascoyne, P.R.C. (1997). Introducing dielectrophoresis as a new force field for field-flow fractionation. *Biophysical Journal* 72 (2): 1118–1129. https://doi.org/10.1016/S0006-3495(97)78144-X.

Ivory, C.F., Gilmartin, M., Gobie, W.A. et al. (1995). A hybrid centrifuge rotor for continuous bioprocessing. *Biotechnology Progress* 11 (1): 21–32. https://doi.org/10.1021/bp00031a003.

Janča, J. and Audebert, R. (1993). New concept in focusing field-flow fractionation and thin layer isopycnic focusing: coupling of primary electric field with secondary gravitational force. *Mikrochimica Acta* 111 (4–6): 163–175. https://doi.org/10.1007/BF01245303.

Janča, J. and Audebert, R. (1994). Experimental study of isopycnic focusing generated by coupled electric and gravitational field forces: use in thin layer focusing and focusing field-flow fractionation. *Mikrochimica Acta* 113 (3–6): 299–311. https://doi.org/10.1007/BF01243620.

Janča, J. (2002a). Micro-channel thermal field-flow fractionation: analysis of ultra-high molar mass polymers and colloidal particles with constant and programmed field force operation. *Journal of Liquid Chromatography & Related Technologies* 25 (13–15): 2173–2191. https://doi.org/10.1081/JLC-120014000.

Janča, J. (2002b). Micro-channel thermal field-flow fractionation: new challenge in analysis of macromolecules and particles. *Journal of Liquid Chromatography and Related Technologies* 25 (5): 683–704. https://doi.org/10.1081/JLC-120003028.

Janča, J., Berneron, J.-F., and Boutin, R. (2003). Micro-thermal field-flow fractionation: new high-performance method for particle size distribution analysis. *Journal of Colloid and Interface Science* 260 (2): 317–323. https://doi.org/10.1016/S0021-9797(02)00216-3.

Janča, J. (2008). *Microthermal Field-Flow Fractionation: Analysis of Synthetic, Natural, and Biological Macromolecules and Particles*. New York: HNB Publishing.

Johann, C., Elsenberg, S., Schuch, H., and Rösch, U. (2015). A novel instrument and method to determine the electrophoretic mobility of nanoparticles and proteins by combining electrical and flow field-flow fractionation. *Analytical Chemistry* 87 (8): 4292–4298. https://doi.org/10.1021/ac504712n.

Kantak, A., Merugu, S., and Gale, B.K. (2006). Improved theory of cyclical electrical field flow fractionation. *Electrophoresis* 27 (14): 2833–2843. https://doi.org/10.1002/elps.200500831.

Karki, K.C., Whitby, E.R., Patankar, S.V. et al. (2001). A numerical model for magnetic chromatography. *Applied Mathematical Modelling* 25 (5): 355–373. https://doi.org/10.1016/S0307-904X(00)00057-3.

Kato, H., Nakamura, A., and Banno, H. (2019). Determination of number-based size distribution of silica particles using centrifugal field-flow fractionation. *Journal of Chromatography A* 1602: 409–418. https://doi.org/10.1016/j.chroma.2019.05.055.

Kesner, L.F., Caldwell, K.D., Myers, M.N., and Giddings, J.C. (1976). Performance characteristics of electrical field-flow fractionation in a flexible membrane channel. *Analytical Chemistry* 48 (13): 1834–1839. https://doi.org/10.1021/ac50007a007.

Kim, Y.B., Yang, J.S., and Moon, M.H. (2018). Investigation of steric transition with field programming in frit inlet asymmetrical flow field-flow fractionation. *Journal of Chromatography A* 1576: 131–136. https://doi.org/10.1016/j.chroma.2018.09.036.

Kohl, Y., Hesler, M., Drexel, R. et al. (2021). Influence of physicochemical characteristics and stability of gold and silver nanoparticles on biological effects and translocation across an intestinal barrier – a case study from in vitro to in silico. *Nanomaterials* 11 (6): 1358. https://doi.org/10.3390/nano11061358.

Lao, A.I.K., Trau, D., and Hsing, I.-M. (2002). Miniaturized flow fractionation device assisted by a pulsed electric field for nanoparticle separation. *Analytical Chemistry* 74 (20): 5364–5369. https://doi.org/10.1021/ac0257647.

Latham, A.H., Freitas, R.S., Schiffer, P., and Williams, M.E. (2005). Capillary magnetic field flow fractionation and analysis of magnetic nanoparticles. *Analytical Chemistry* 77 (15): 5055–5062. https://doi.org/10.1021/ac050611f.

Lee, H.-L., Reis, J.F.G., Dohner, J., and Lightfoot, E.N. (1974). Single-phase chromatography: solute retardation by ultrafiltration and electrophoresis. *AIChE Journal* 20 (4): 776–784. https://doi.org/10.1002/aic.690200420.

Lee, H., Kim, H., and Moon, M.H. (2005). Field programming in frit inlet asymmetrical flow field-flow fractionation/multiangle light scattering: application to sodium hyaluronate. *Journal of Chromatography A* 1089 (1–2): 203–210. https://doi.org/10.1016/j.chroma.2005.06.069.

Lee, H.L. and Lightfoot, E.N. (1976). Preliminary report on ultrafiltration-induced polarization chromatography – an analog of field-flow fractionation. *Separation Science* 11 (5): 417–440. https://doi.org/10.1080/01496397608085333.

Lee, S., Myers, M.N., Beckett, R., and Giddings, J.C. (1988). Particle separation and characterization by sedimentation/cyclical-field field-flow fractionation. *Analytical Chemistry* 60 (11): 1129–1135. https://doi.org/10.1021/ac00162a009.

Lee, S., Myers, M.N., and Giddings, J.C. (1989). Hydrodynamic relaxation using stopless flow injection in split inlet sedimentation field-flow fractionation. *Analytical Chemistry* 61 (21): 2439–2444. https://doi.org/10.1021/ac00196a023.

Lee, W.J., Min, B.-R., and Moon, M.H. (1999). Improvement in particle separation by hollow fiber flow field-flow fractionation and the potential use in obtaining particle size distribution. *Analytical Chemistry* 71 (16): 3446–3452. https://doi.org/10.1021/ac981204p.

Lightfoot, E.N., Noble, P.T., Chiang, A.S., and Ugulini, T.A. (1981). Characterization of an improved electropolarization chromatographic system using homogenous proteins. *Separation Science and Technology* 16 (6): 619–656. https://doi.org/10.1080/01496398108058120.

Litzén, A. and Wahlund, K.-G. (1991). Zone broadening and dilution in rectangular and trapezoidal asymmetrical flow field-flow fractionation channels. *Analytical Chemistry* 63 (10): 1001–1007. https://doi.org/10.1021/ac00010a013.

Litzén, A. (1993). Separation speed, retention, and dispersion in asymmetrical flow field-flow fractionation as functions of channel dimensions and flow rates. *Analytical Chemistry* 65 (4): 461–470. https://doi.org/10.1021/ac00052a025.

Litzén, A., Walter, J.K., Krischollek, H., and Wahlund, K.-G. (1993). Separation and quantitation of monoclonal antibody aggregates by asymmetrical flow field-flow fractionation and comparison to gel permeation chromatography. *Analytical Biochemistry* 212 (2): 469–480. https://doi.org/10.1006/abio.1993.1356.

Liu, G. and Giddings, J.C. (1991). Separation of particles in nonaqueous suspensions by thermal-electrical field-flow fractionation. *Analytical Chemistry* 63 (3): 296–299. https://doi.org/10.1021/ac00003a021.

Liu, G. and Giddings, J.C. (1992). Separation of particles in aqueous suspensions by thermal field-flow fractionation. Measurement of thermal diffusion coefficients. *Chromatographia* 34 (9–10): 483–492. https://doi.org/10.1007/BF02290241.

Liu, M.-K., Williams, P.S., Myers, M.N., and Giddings, J.C. (1991). Hydrodynamic relaxation in flow field-flow fractionation using both split and frit inlets. *Analytical Chemistry* 63 (19): 2115–2122. https://doi.org/10.1021/ac00019a010.

Markx, G.H., Rousselet, J., and Pethig, R. (1997). DEP-FFF: field-flow fractionation using non-uniform electric fields. *Journal of Liquid Chromatography & Related Technologies* 20 (16–17): 2857–2872. https://doi.org/10.1080/10826079708005597.

Martin, M. and Giddings, J.C. (1981). Retention and nonequilibrium peak broadening for a generalized flow profile in field-flow fractionation. *Journal of Physical Chemistry* 85 (6): 727–733. https://doi.org/10.1021/j150606a025.

Martin, M. (1996). Relative velocity profile and flow-rate in sedimentation field-flow fractionation. *Journal of High Resolution Chromatography & Chromatography Communications* 19 (9): 481–484. https://doi.org/10.1002/jhrc.1240190902.

Martin, M. (1997). Time-based retention ratio for curved separation channels: application to sedimentation field-flow fractionation. *Journal of Microcolumn Separations* 9 (3): 225–232. https://doi.org/10.1002/(SICI)1520-667X(1997)9:3<225::AID-MCS11>3.0.CO;2-7.

Martin, M. (1998). Theory of field-flow fractionation. In: *Advances in Chromatography*, vol. 39, Ch. 1 (ed. P.R. Brown and E. Grusha), 1–138. New York: Marcel Dekker Inc.

Martin, M., van Batten, C., and Hoyos, M. (2002). Determination of thermodiffusion parameters from thermal field-flow fractionation retention data. In: *Thermal Nonequilibrium Phenomena in Liquid Mixtures*, vol. 584, Ch. 13 (ed. W. Köhler and S. Wiegand), 250–284. Berlin, Heidelberg: Springer https://doi.org/10.1007/3-540-45791-7_13.

Martin, M. and Hoyos, M. (2011). On the no-field method for void time determination in flow field-flow fractionation. *Journal of Chromatography A* 1218 (27): 4117–4125. https://doi.org/10.1016/j.chroma.2011.01.010.

Martin, M. and Williams, P.S. (1992). Theoretical basis of field-flow fractionation. In: *Theoretical Advancement in Chromatography and Related Techniques, NATO ASI Series C: Mathematical and Physical Sciences*, vol. 383 (ed. F. Dondi and G. Guiochon), 513–580. Dordrecht, The Netherlands: Kluwer Academic Publisher https://doi.org/10.1007/978-94-011-2686-1_18.

Messaud, F.A., Sanderson, R.D., Runyon, J.R. et al. (2009). An overview on field-flow fractionation techniques and their applications in the separation and characterization of polymers. *Progress in Polymer Science* 34 (4): 351–368. https://doi.org/10.1016/j.progpolymsci.2008.11.001.

Metzger, C., Drexel, R., Meier, F., and Briesen, H. (2021). Effect of ultrasonication on the size distribution and stability of cellulose nanocrystals in suspension: an asymmetrical flow field-flow fractionation study. *Cellulose* 28: 10221–10238. https://doi.org/10.1007/s10570-021-04172-3.

Min, B.R., Kim, S.J., Ahn, K.-H., and Moon, M.H. (2002). Hyperlayer separation in hollow fiber flow field-flow fractionation: effect of membrane materials on resolution and selectivity. *Journal of Chromatography A* 950 (1–2): 175–182. https://doi.org/10.1016/S0021-9673(02)00029-8.

Mitsuhashi, K., Yoshizaki, R., Ohara, T. et al. (2002). Retention of ions in a magnetic chromatograph using high-intensity and high-gradient magnetic fields. *Separation Science and Technology* 37 (16): 3635–3645. https://doi.org/10.1081/SS-120014810.

Moon, M.H. (1995). Effect of carrier solutions on particle retention in flow field-flow fractionation. *Bulletin of the Korean Chemical Society* 16 (7): 613–619. https://doi.org/10.5012/bkcs.1995.16.7.613.

Moon, M.H., Kwon, H., and Park, I. (1997). Stopless flow injection in asymmetrical flow field-flow fractionation using a frit inlet. *Analytical Chemistry* 69 (7): 1436–1440. https://doi.org/10.1021/ac960897b.

Moon, M.H., Williams, P.S., and Kwon, H. (1999). Retention and efficiency in frit-inlet asymmetrical flow field-flow fractionation. *Analytical Chemistry* 71 (14): 2657–2666. https://doi.org/10.1021/ac990040p.

Moon, M.H. (2001). Frit-inlet asymmetrical flow field-flow fractionation (FI-AFlFFF): a stopless separation technique for macromolecules and nanoparticles. *Bulletin of the Korean Chemical Society* 22 (4): 337–348. https://doi.org/10.5012/bkcs.2001.22.4.337.

Moon, M.H., Williams, P.S., Kang, D., and Hwang, I. (2002). Field and flow programming in frit-inlet asymmetrical flow field-flow fractionation. *Journal of Chromatography A* 955 (2): 263–272. https://doi.org/10.1201/b11760-16.

Mori, S. (1986). Magnetic field-flow fractionation using capillary tubing. *Chromatographia* 21 (11): 642–644. https://doi.org/10.1007/BF02311919.

Myers, M.N., Caldwell, K.D., and Giddings, J.C. (1974). A study of retention in thermal field-flow fractionation. *Separation Science* 9 (1): 47–70. https://doi.org/10.1080/01496397408080043.

Myers, M.N. and Giddings, J.C. (1979). A continuous steric FFF device for the size separation of particles. *Powder Technology* 23 (1): 15–20. https://doi.org/10.1016/0032-5910(79)85021-4.

Nickel, C., Scherer, C., Noskov, S. et al. (2021). Observation of interaction forces by investigation of the influence of eluent additives on the retention behavior of aqueous nanoparticle dispersions in asymmetrical flow field-flow fractionation. *Journal of Chromatography A* 1637: 461840. https://doi.org/10.1016/j.chroma.2020.461840.

Nomizu, T., Yamamoto, K.-i., and Watanabe, M. (2001). Magnetic chromatography for magnetic fine particles using a periodically intermittent magnetic field. *Analytical Sciences* 17: i177–i180. https://doi.org/10.14891/analscisp.17icas.0.i177.0.

Oberteuffer, J.A. (1973). High gradient magnetic separation. *IEEE Transactions on Magnetics* 9 (3): 303–306. https://doi.org/10.1109/TMAG.1973.1067673.

Ohara, T., Mori, S., Oda, Y. et al. (1996). Feasibility of magnetic chromatography for ultra-fine particle separation. *Transactions of the IEE Japan* 116 (8): 979–986. https://doi.org/10.1541/ieejpes1990.116.8_979.

Ohara, T. (1997). Feasibility of using magnetic chromatography for ultra-fine particle separation. In: *High Magnetic Fields: Applications, Generations, Materials* (ed. H.J. Schneider-Muntau), 43–55. Hackensack, NJ: World Scientific.

Ohara, T., Wang, X., Wada, H., and Whitby, E.R. (2000). Magnetic chromatography: numerical analysis in the case of particle size distribution. *Transactions of the IEE Japan* 120 (1): 62–67. https://doi.org/10.1541/ieejfms1990.120.1_62.

Ornthai, M., Siripinyanond, A., and Gale, B.K. (2015). Biased cyclical electrical field-flow fractionation for separation of submicron particles. *Analytical and Bioanalytical Chemistry* 408 (3): 855–863. https://doi.org/10.1007/s00216-015-9173-5.

Palkar, S.A. and Schure, M.R. (1997a). Mechanistic study of electrical field flow fractionation. 1. Nature of the internal field. *Analytical Chemistry* 69 (16): 3223–3229. https://doi.org/10.1021/ac9700134.

Palkar, S.A. and Schure, M.R. (1997b). Mechanistic study of electrical field flow fractionation. 2. Effect of sample conductivity on retention. *Analytical Chemistry* 69 (16): 3230–3238. https://doi.org/10.1021/ac970014w.

Park, M.R., Kang, D.Y., Chmelik, J. et al. (2008). Different elution modes and field programming in gravitational field-flow fractionation: effect of channel angle. *Journal of Chromatography A* 1209 (1–2): 206–211. https://doi.org/10.1016/j.chroma.2008.09.014.

Pearlstein, A.J. and Shiue, M.-P. (1995). Three-dimensional field-flow fractionation using helical flow. *Separation Science and Technology* 30 (11): 2251–2258. https://doi.org/10.1080/01496399508013110.

Plocková, J. and Chmelík, J. (2000). Different elution modes and field programming in gravitational field-flow fractionation. 2. Experimental verification of the range of conditions for flow-rate and carrier liquid density programming. *Journal of Chromatography A* 868 (2): 217–227. https://doi.org/10.1016/S0021-9673(99)01235-2.

Plocková, J. and Chmelík, J. (2001). Different elution modes and field programming in gravitational field-flow fractionation. III. Field programming by flow-rate gradient generated by a programmable pump. *Journal of Chromatography A* 918 (2): 361–370. https://doi.org/10.1016/S0021-9673(01)00706-3.

Plocková, J., Matulík, F., and Chmelík, J. (2002). Different elution modes and field programming in gravitational field-flow fractionation. IV. Field programming achieved with channels of non-constant cross-sections. *Journal of Chromatography A* 955 (1): 95–103. https://doi.org/10.1016/S0021-9673(02)00195-4.

Plocková, J. and Chmelík, J. (2006). Different elution modes and field programming in gravitational field-flow fractionation: field programming using density and viscosity gradients. *Journal of Chromatography A* 1118 (2): 253–260. https://doi.org/10.1016/j.chroma.2006.03.124.

Reis, J.F.G. and Lightfoot, E.N. (1976). Electropolarization chromatography. *AIChE Journal* 22 (4): 779–785. https://doi.org/10.1002/aic.690220423.

Reis, J.F.G., Ramkrishna, D., and Lightfoot, E.N. (1978). Convective mass transfer in the presence of polarizing fields: dispersion in hollow fiber electropolarization chromatography. *AIChE Journal* 24 (4): 679–686. https://doi.org/10.1002/aic.690240416.

Schimpf, M.E. and Giddings, J.C. (1989). Characterization of thermal diffusion in polymer solutions by thermal field-flow fractionation: dependence on polymer and solvent parameters. *Journal of Polymer Science: Part B: Polymer Physics* 27 (6): 1317–1332. https://doi.org/10.1002/polb.1989.090270610.

Schimpf, M.E. and Wahlund, K.-G. (1997). Asymmetrical flow field-flow fractionation as a method to study the behavior of humic acids in solution. *Journal of Microcolumn Separations* 9 (7): 535–543. https://doi.org/10.1002/(SICI)1520-667X(1997)9:7<535::AID-MCS3>3.0.CO;2-2.

Schimpf, M.E. and Semenov, S.N. (2000). Mechanism of polymer thermophoresis in nonaqueous solvents. *The Journal of Physical Chemistry B* 104 (42): 9935–9942. https://doi.org/10.1021/jp994334q.

Schunk, T.C., Gorse, J., and Burke, M.F. (1984). Parameters affecting magnetic field-flow fractionation of metal oxide particles. *Separation Science and Technology* 19 (10): 653–666. https://doi.org/10.1080/01496398408060667.

Schure, M.R., Myers, M.N., Caldwell, K.D. et al. (1985). Separation of coal fly ash using continuous steric field-flow fractionation. *Environmental Science and Technology* 19 (8): 686–689. https://doi.org/10.1021/es00138a005.

Schure, M.R. and Weeratunga, S.K. (1991). Coriolis-induced secondary flow in sedimentation field-flow fractionation. *Analytical Chemistry* 63 (22): 2614–2626. https://doi.org/10.1021/ac00022a015.

Semenov, S.N. (1986). Flow fractionation in a strong transverse magnetic field. *Russian Journal of Physical Chemistry* 60 (5): 729–731.

Semenov, S.N. and Kuznetsov, A.A. (1986). Flow fractionation in a transverse high-gradient magnetic field. *Russian Journal of Physical Chemistry* 60 (2): 247–250.

Semenov, S.N. and Schimpf, M.E. (2020). Comparative examination of nonequilibrium thermodynamic models of thermodiffusion in liquids. *Proceedings* 46 (1): 14. https://doi.org/10.3390/ecea-5-06680.

Shah, A.B., Reis, J.F.G., Lightfoot, E.N., and Moore, R.E. (1979). Modeling electroretention of proteins during electropolarization chromatography. *Separation Science and Technology* 14 (6): 475–497. https://doi.org/10.1080/01496397908068471.

Shiundu, P.M., Liu, G., and Giddings, J.C. (1995). Separation of particles in nonaqueous suspensions by thermal field-flow fractionation. *Analytical Chemistry* 67 (15): 2705–2713. https://doi.org/10.1021/ac00111a032.

Shiundu, P.M., Munguti, S.M., and Williams, S.K.R. (2003). Retention behavior of metal particle dispersions in aqueous and nonaqueous carriers in thermal field-flow fractionation. *Journal of Chromatography A* 983 (1–2): 163–176. https://doi.org/10.1016/S0021-9673(02)01694-1.

Srinivas, M., Sant, H.J., and Gale, B.K. (2010). Optimization of cyclical electrical field flow fractionation. *Electrophoresis* 31 (20): 3372–3379. https://doi.org/10.1002/elps.201000024.

Stevens, F.J. (1990). Fractionation of macromolecules in an alternating transverse electric field: simulation of the method. *Journal of Biochemical and Biophysical Methods* 20 (4): 275–292. https://doi.org/10.1016/0165-022X(90)90090-Y.

Takahashi, M., Fukui, S., Takahashi, Y. et al. (2006). Numerical study on magnetic chromatography using quadrupole magnetic field. *IEEE Transactions on Applied Superconductivity* 16 (2): 1116–1119. https://doi.org/10.1109/TASC.2006.871336.

Tasci, T.O., Johnson, W.P., Fernandez, D.P. et al. (2013). Biased cyclical electrical field flow fractionation for separation of sub 50 nm particles. *Analytical Chemistry* 85 (23): 11225–11232. https://doi.org/10.1021/ac401331z.

Thompson, G.H., Myers, M.N., and Giddings, J.C. (1967). An observation of a field-flow fractionation effect with polystyrene samples. *Separation Science* 2 (6): 797–900. https://doi.org/10.1080/01496396708049739.

Thompson, G.H., Myers, M.N., and Giddings, J.C. (1969). Thermal field-flow fractionation of polystyrene samples. *Analytical Chemistry* 41 (10): 1219–1222. https://doi.org/10.1021/ac60279a001.

Tri, N., Caldwell, K., and Beckett, R. (2000). Development of electrical field-flow fractionation. *Analytical Chemistry* 72 (8): 1823–1829. https://doi.org/10.1021/ac990822i.

Tsukamoto, O., Ohizumi, T., Ohara, T. et al. (1995). Feasibility study on separation of several tens nanometer scale particles by magnetic field-flow-fractionation technique using superconducting magnet. *IEEE Transactions on Applied Superconductivity* 5 (2): 311–314. https://doi.org/10.1109/77.402551.

van Asten, A.C., Boelens, H.F.M., Kok, W.T. et al. (1994). Temperature dependence of solvent viscosity, solvent thermal conductivity, and Soret coefficient in thermal field-flow fractionation. *Separation Science and Technology* 29 (4): 513–533. https://doi.org/10.1080/01496399408002159.

Vastamäki, P., Jussila, M., and Riekkola, M.-L. (2001). Development of continuously operating two-dimensional thermal field-flow fractionation equipment. *Separation Science and Technology* 36 (11): 2535–2545. https://doi.org/10.1081/SS-100106108.

Vastamäki, P., Jussila, M., and Riekkola, M.-L. (2003). Study of continuous two-dimensional thermal field-flow fractionation of polymers. *The Analyst* 128 (10): 1243–1248. https://doi.org/10.1039/b307292b.

Vastamäki, P., Jussila, M., and Riekkola, M.-L. (2005). Continuous two-dimensional field-flow fractionation: a novel technique for continuous separation and collection of macromolecules and particles. *The Analyst* 130 (4): 427–432. https://doi.org/10.1039/b410046h.

Vastamäki, P., Williams, P.S., Matti, J. et al. (2014). Retention in continuous two-dimensional thermal field-flow fractionation: comparison of experimental results with theory. *The Analyst* 139 (1): 116–127. https://doi.org/10.1039/C3AN01047C.

Vauthier, J.-C. and Williams, P.S. (1998). Numerical simulation of band-broadening during hydrodynamic relaxation in frit-inlet field-flow fractionation channels. *Journal of Chromatography A* 805 (1–2): 149–160. https://doi.org/10.1016/S0021-9673(98)00009-0.

Vickrey, T.M. and Garcia-Ramirez, J.A. (1980). Magnetic field-flow fractionation: theoretical basis. *Separation Science and Technology* 15 (6): 1297–1304. https://doi.org/10.1080/01496398008068506.

Wahlund, K.-G., Winegarner, H.S., Caldwell, K.D., and Giddings, J.C. (1986). Improved flow field-flow fractionation system applied to water soluble polymers: programming, outlet stream splitting, and flow optimization. *Analytical Chemistry* 58 (3): 573–578. https://doi.org/10.1021/ac00294a018.

Wahlund, K.-G. and Giddings, J.C. (1987). Properties of an asymmetrical flow field-flow fractionation channel having one permeable wall. *Analytical Chemistry* 59 (9): 1332–1339. https://doi.org/10.1021/ac00136a016.

Wahlund, K.-G. and Litzén, A. (1989). Application of an asymmetrical flow field-flow fractionation channel to the separation and characterization of proteins, plasmids, plasmid fragments, polysaccharides and unicellular algae. *Journal of Chromatography* 461: 73–87. https://doi.org/10.1016/S0021-9673(00)94276-6.

Wahlund, K.-G. (2013). Flow field-flow fractionation: critical overview. *Journal of Chromatography A* 1287: 97–112. https://doi.org/10.1016/j.chroma.2013.02.028.

Wang, X.-B., Vykoukal, J., Becker, F.F., and Gascoyne, P.R.C. (1998). Separation of polystyrene microbeads using dielectrophoretic/gravitational field-flow-fractionation. *Biophysical Journal* 74 (5): 2689–2701. https://doi.org/10.1016/S0006-3495(98)77975-5.

Wang, X.-B., Yang, J., Huang, Y. et al. (2000). Cell separation by dielectrophoretic field-flow-fractionation. *Analytical Chemistry* 72 (4): 832–839. https://doi.org/10.1021/ac990922o.

Wang, X., Ohara, T., Whitby, E.R. et al. (1997). Computer simulation of magnetic chromatography system for ultra-fine particle separation. *Transactions of the IEE Japan* 117 (11): 1466–1474. https://doi.org/10.1541/ieejpes1990.117.11_1466.

Williams, P.S. and Giddings, J.C. (1987). Power programmed field-flow fractionation: a new program form for improved uniformity of fractionating power. *Analytical Chemistry* 59 (17): 2038–2044. https://doi.org/10.1021/ac00144a007.

Williams, P.S., Giddings, J.C., and Beckett, R. (1987). Fractionating power in sedimentation field-flow fractionation with linear and parabolic field decay programming. *Journal of Liquid Chromatography* 10 (8–9): 1961–1998. https://doi.org/10.1080/01483918708066808.

Williams, P.S., Koch, T., and Giddings, J.C. (1992). Characterization of near-wall hydrodynamic lift forces using sedimentation field-flow fractionation. *Chemical Engineering Communications* 111: 121–147. https://doi.org/10.1080/00986449208935984.

Williams, P.S. and Giddings, J.C. (1994). Theory of field-programmed field-flow fractionation with corrections for steric effects. *Analytical Chemistry* 66 (23): 4215–4228. https://doi.org/10.1021/ac00095a017.

Williams, P.S., Lee, S., and Giddings, J.C. (1994). Characterization of hydrodynamic lift forces by field-flow fractionation. Inertial and near-wall lift forces. *Chemical Engineering Communications* 130 (1): 143–166. https://doi.org/10.1080/00986449408936272.

Williams, P.S., Moon, M.H., and Giddings, J.C. (1996a). Influence of accumulation wall and carrier solution composition on lift force in sedimentation/steric field-flow fractionation. *Colloids and Surfaces A: Physicochemical and Engineering Aspects* 113 (3): 215–228. https://doi.org/10.1016/0927-7757(96)03669-2.

Williams, P.S., Moon, M.H., Xu, Y., and Giddings, J.C. (1996b). Effect of viscosity on retention time and hydrodynamic lift forces in sedimentation/steric field-flow fractionation. *Chemical Engineering Science* 51 (19): 4477–4488. https://doi.org/10.1016/0009-2509(96)00291-6.

Williams, P.S. (1997). Design of an asymmetrical flow field-flow fractionation channel for uniform channel flow velocity. *Journal of Microcolumn Separations* 9 (6): 459–467. https://doi.org/10.1002/(SICI)1520-667X(1997)9:6<459::AID-MCS3>3.0.CO;2-0.

Williams, P.S. (2022). Theoretical principles of field-flow fractionation and SPLITT fractionation. In: *Particle Separation Techniques* (ed. C. Contado), 579–620. Amsterdam, The Netherlands: Elsevier https://doi.org/10.1016/B978-0-323-85486-3.00001-9.

Williams, P.S., Xu, Y., Reschiglian, P., and Giddings, J.C. (1997). Colloid characterization by sedimentation field-flow fractionation: correction for particle-wall interaction. *Analytical Chemistry* 69 (3): 349–360. https://doi.org/10.1021/ac9606012.

Williams, P.S. (2000a). Programmed field-flow fractionation: fractionating power and optimization. In: *Field-Flow Fractionation Handbook*. (Ch 10 (ed. M.E. Schimpf, K. Caldwell, and J.C. Giddings), 167–182. New York, NY: Wiley-Interscience.

Williams, P.S., Giddings, M.C., and Giddings, J.C. (2001). A data analysis algorithm for programmed field-flow fractionation. *Analytical Chemistry* 73 (17): 4202–4211. https://doi.org/10.1021/ac010305b.

Williams, P.S., Carpino, F., and Zborowski, M. (2009a). Theory for nanoparticle retention time in the helical channel of quadrupole magnetic field-flow fractionation. *Journal of Magnetism and Magnetic Materials* 321 (10): 1446–1451. https://doi.org/10.1016/j.jmmm.2009.02.065.

Williams, P.S., Carpino, F., and Zborowski, M. (2009b). Magnetic nanoparticle drug carriers and their study by quadrupole magnetic field-flow fractionation. *Molecular Pharmaceutics* 6 (5): 1290–1306. https://doi.org/10.1021/mp900018v.

Williams, P.S., Carpino, F., Moore, L.R., and Zborowski, M. (2010a). Magnetic field programming in quadrupole magnetic field-flow fractionation. *Physics Procedia* 9: 91–95. https://doi.org/10.1016/j.phpro.2010.11.022.

Williams, P.S., Carpino, F., and Zborowski, M. (2010b). Erratum to: "Theory for nanoparticle retention time in the helical channel of quadrupole magnetic field-flow fractionation" [J. Magn. Magn. Mater. 321 (2009) 1446–1451]. *Journal of Magnetism and Magnetic Materials* 322 (21): 3605. https://doi.org/10.1016/j.jmmm.2010.07.011.

Williams, P.S., Carpino, F., and Zborowski, M. (2010c). Characterization of magnetic nanoparticles using programmed quadrupole magnetic field-flow fractionation. *Philosophical Transactions of the Royal Society A: Mathematical, Physical & Engineering Sciences* 368 (1927): 4419–4437. https://doi.org/10.1098/rsta.2010.0133.

Williams, P.S. (2012). Separation and characterization of magnetic particulate materials. In: *Magnetic Nanoparticles: From Fabrication to Clinical Applications* (Ch. 11 (ed. N.T.K. Thanh), 301–332. Boca Raton, FL: CRC Press https://doi.org/10.1201/b11760-16.

Williams, P.S. (2015). Retention ratio and nonequilibrium bandspreading in asymmetrical flow field-flow fractionation. *Analytical and Bioanalytical Chemistry* 407 (15): 4327–4338. https://doi.org/10.1007/s00216-015-8734-y.

Williams, P.S. (2016). Fractionating power and outlet stream polydispersity in asymmetrical flow field-flow fractionation. Part I: isocratic operation. *Analytical and Bioanalytical Chemistry* 408 (12): 3247–3263. https://doi.org/10.1007/s00216-016-9388-0.

Williams, P.S. (2017). Fractionating power and outlet stream polydispersity in asymmetrical flow field-flow fractionation. Part II: programmed operation. *Analytical and Bioanalytical Chemistry* 409 (1): 317–334. https://doi.org/10.1007/s00216-016-0007-x.

Williams, P.S. (2024). Correction to: Fractionating power and outlet stream polydispersity in asymmetrical flow field-flow fractionation. Part II: programmed operation. *Analytical and Bioanalytical Chemistry* 416 (28): 6687–6689. https://doi.org/10.1007/s00216-024-05527-y.

Williams, S.K.R. (2000b). Sample recovery. In: *Field-Flow Fractionation Handbook* (Ch. 21 (ed. M.E. Schimpf, K. Caldwell, and J.C. Giddings), 325–343. New York: Wiley-Interscience.

Yang, J., Huang, Y., Wang, X.-B. et al. (2000). Differential analysis of human leukocytes by dielectrophoretic field-flow-fractionation. *Biophysical Journal* 78 (5): 2680–2689. https://doi.org/10.1016/S0006-3495(00)76812-3.

Yin, H.-Y., Zuo, C.-C., and Shi, H.-Y. (2013). Fabrication of ultrasound-gravity field flow fractionation devices using engraving machine and reliable sealing method. *Advanced Materials Research* 748: 765–768. https://doi.org/10.4028/www.scientific.net/AMR.748.765.

You, Z., Meier, F., and Weidner, S. (2017). Comparison of miniaturized and conventional asymmetrical flow field-flow fractionation (AF4) channels for nanoparticle separations. *Separations* 4 (1): 8. https://doi.org/10.3390/separations4010008.

Zheng, F. (2002). Thermophoresis of spherical and non-spherical particles: a review of theories and experiments. *Advances in Colloid and Interface Science* 97 (1–3): 255–278. https://doi.org/10.1016/S0001-8686(01)00067-7.